Sting jets in extratropical cyclones: a review

Received: 27 June 2017 | Revised: 25 January 2018 | Accepted: 07 February 2018 | Published on: 31 August 2018

DOI: 10.1002/qj.3267

REVIEW ARTICLE

Quarterly Journal of the Royal Meteorological Society RMetS

Sting jets in extratropical cyclones: a review

Peter A. Clark | Suzanne L. Gray

Department of Meteorology, University of Reading, UK

Correspondence
Peter A. Clark, Department of Meteorology, University of Reading, Earley Gate, PO Box 243, Reading RG6 6BB, UK. Email: p.clark@reading.ac.uk

Funding information
Natural Environment Research Council grant NE/E004415/1 and the AXA Research Fund.

This article reviews the current state of knowledge of sting jets (SJs) in extratropical cyclones. SJs were formally identified in 2004 by the pioneering work of Keith Browning. Reviewing this and subsequent studies, we define the SJ as a coherent air flow that descends from mid-levels inside the cloud head into the frontal-fracture region of a Shapiro–Keyser cyclone over a period of a few hours leading to a distinct region of near-surface stronger winds. It therefore lies above the cold conveyor belt during some stage of its life, but, at least in some cases, descends to reach the top of boundary layer ahead of the cold conveyor belt. It is not attributed to a specific mechanism in this definition. We conclude that it is likely that a continuum of SJ descent and speed-up mechanisms exists. At one extreme is balanced descent partly associated with frontolysis in the frontal-fracture region. More horizontally small-scale and stronger frontolytic descent may occur associated with weak stability to slantwise convective downdraughts. Instability to slantwise convective downdraughts may occur in some systems, leading to multiple slantwise convective downdraughts associated with the release of conditional symmetric instability and even, possibly, symmetric instability. The global climatology of SJs and the interaction between the atmospheric boundary layer and SJs are revealed as specific areas where more research is needed. Finally, we describe eight myths and misunderstandings that exist in the current literature with the aim of guiding future research into the SJ phenomenon.

KEYWORDS
cyclone, extratropical, gust, jet, sting, wind

1 | INTRODUCTION

Extratropical cyclones (ETCs) are a major cause of hazardous weather, primarily in the form of wind and rain or snow fall (e.g. windstorm insured-loss estimations in the Extreme Windstorm Catalogue: http://www.europeanwindstorms.org, in which the largest insured loss of $8.2bn (indexed to 2012 values) is for the 1990 windstorm *Daria*). The precise location, timing and degree of impact depends upon the mesoscale structure of the cyclone. This structure is complex and involves the combination of many processes. However, many features, such as fronts, are common to many, if not all, ETCs, and conceptual models have been developed and refined over many decades to help identify and understand some of these key features (collections edited by Newton and Holopainen (1990) and Shapiro and Grønås (1999)). Such conceptual models help the forecaster identify features in observations and recognise risk where and when observations are not available. They also form a valuable test of numerical models, which may be unable to reproduce some key features due to limitations of resolution or model physics.

The "Great Storm" of October 16, 1987 was a particularly damaging ETC. An estimated 15 million trees were blown down, representing 3.9 million cubic metres of timber (Grayson, 1989), and 22 people lost their lives. The peak winds occurring over southeast England were estimated to

have a return period of 200 years (Met Office Advisory Services 1988), and it was probably the most devastating storm in the region since 1703. Browning (2004) (hereafter referred to as B04) revisited this storm to study the structure of the surface wind field in detail. He identified a number of features. Some features of ETCs are well known, including the "warm conveyor belt" (WCB), associated with persistent, strong winds throughout much of the lifetime of an ETC, the somewhat shorter-lived "cold conveyor belt" (CCB) that often produces strong surface winds as it wraps around the centre of the cyclone, and the "dry intrusion" and "dry slot" region. (section 2.2 gives more detail.) Browning identified strong surface gusts in the "dry slot" region associated with deep convection. Behind this, but ahead of the CCB, he also identified a distinct mesoscale region of extremely strong surface winds and, especially, gusts close to the "tail" of the characteristic "hook" of the cloud head and distinct from both the WCB and the CCB. This region of gusts was responsible for most of the damage caused by the storm. He dubbed this mesoscale strong wind region "the sting at the end of the tail." This phrase relates the jet as being at the end of (i.e. beyond) the "poisonous tail" of the bent-back front, an analogy to a scorpion curved around the low-pressure centre of the storm. In the final sentence of the conclusions of B04, the contraction "Sting Jet" (SJ) is used, terminology that has endured. B04 defined the SJ as air that "leaves the hooked tip of the cloud head (and enters the dry slot) much faster than the rate of travel of the cloud-head tip." The terminology "poisonous tail" is taken from Grønås (1995) which actually says

"As a young forecaster in the late 1960s, I was informed that the strongest winds ever recorded in our region have been linked to bent-back occlusions. Such a structure has been called the 'poisonous tail' of the bent-back occlusion (after F. Spinnangr)…."

The structure studied in the article is probably primarily the CCB; the horizontal grid-length of the model used (50 km) is insufficient to make a clear identification. However, it seems very possible that the forecaster experience referred to included the surface impacts of SJs.

The term SJ also alludes to its relatively short-lived nature (especially at the ground) compared with, for example, the WCB and CCB. This presents a forecasting challenge even today, as direct evidence (in terms of surface wind) of its presence may not be available until the last minute. Nevertheless, awareness of the existence of SJs is now informing operational forecasting. For example, forecasters in the UK Met Office inferred the presence of a SJ from high-resolution (1.5 km horizontal grid) forecasts in the storm that reached Scotland on December 8, 2011 (windstorm *Friedhelm*) and, as a result, increased the level of official warning from amber to red. Incidentally, these forecasts were used to guide aircraft flight paths through the storm as part of the DIAMET field programme (Baker *et al.*, 2013).

The identification of the SJ stimulated a body of new research which continues today. At present the SJ is far from fully understood. One feature of the SJ which is certain is that not all ETCs develop a SJ. Furthermore, the SJ is not easy to detect with routine observations. This has led to misapprehensions and disagreements in the literature concerning many aspects of the SJ, even regarding its precise definition. In this article we review the current literature with a view to providing a clear statement of what is known and what is not known, and to dispel some of the myths and misunderstandings surrounding the SJ.

This review article is structured as follows. In section 2 we lay the groundwork for the rest of the article by outlining the relevant aspects of cyclone evolution and mesoscale instabilities needed to understand SJs. In section 3 and section 4 the observational and modelling evidence, respectively, for SJs are assessed. In section 5 we synthesise knowledge of the mechanisms that can lead to SJ formation and maintenance. In section 6 and section 7 we review our knowledge of the role of the boundary layer in leading to strong surface winds attributable to SJs and of the climatology of SJs, respectively. In section 8 we list and provide evidence for eight myths and misunderstandings surrounding the SJ. We conclude in section 9.

2 | THE PRE-HISTORY OF STING JETS

The SJ has been identified within cyclones only following the conceptual life-cycle model identified by Shapiro and Keyser (1990). Current hypotheses regarding the mechanism of its formation thus focus on specific characteristics of these cyclones. Furthermore, some hypotheses are based upon the development of mesoscale instabilities that are known to occur in some cyclones. In the following sections we briefly summarize this conceptual and theoretical background to facilitate later discussions.

2.1 | Shapiro–Keyser cyclone evolution

The Norwegian cyclone model has been the primary conceptual model of the structure of ETCs for a century (e.g. Bjerknes, 1919; Bjerknes and Solberg, 1922). Shapiro and Keyser developed a new life-cycle model (abbreviated as the SK evolution in the following text) as representative of marine cyclones and based it on the results of idealized developing baroclinic wave simulations and simulated case-studies as well as observations, including those from the pre-ERICA (Experiment on Rapidly Intensifying Cyclones over the Atlantic) test flights that showed the T-bone phase and frontal fracture.

The SJ has been found in both model simulations and observational analyses to descend from mid-tropospheric levels towards the top of the boundary layer in the frontal-fracture region of intensifying ETCs following the SK conceptual life-cycle model. The four stages of the SK evolution are presented in Figure 1 (adapted from Schultz and Vaughan,

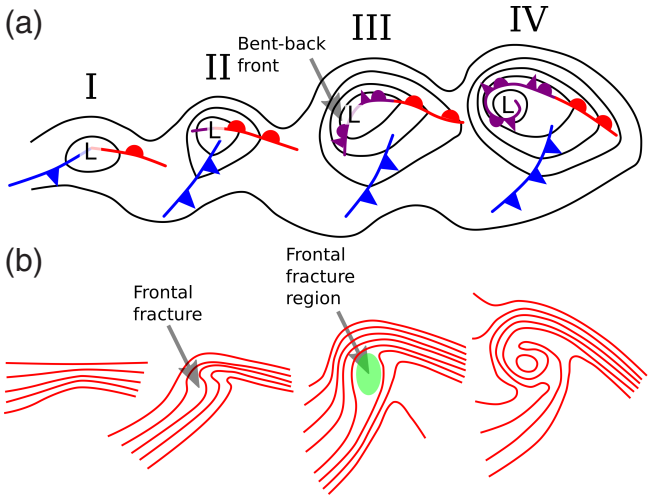

FIGURE 1 Conceptual model of a Shapiro–Keyser cyclone showing (a) lower-tropospheric (e.g. 850 hPa) geopotential height and fronts, and (b) lower-tropospheric potential temperature. The stages in the respective cyclone evolutions are separated by approximately 6 hr and the frontal symbols are conventional. The characteristic scale of the cyclones based on the distance from the geopotential height minimum, denoted by L, to the outermost geopotential height contour in stage IV is 1,000 km. Figure and caption are adapted from Schultz and Vaughan (2011) (their figure 12), which was adapted from Shapiro and Keyser (1990) (their figure 10.27) to enhance the zonal elongation of the cyclone and fronts and to reflect the continued existence of the frontal T-bone in stage IV, and from figure 15b in Schultz *et al.* (1998) to change the back-bent warm front into an occluded front and back-bent occluded front [Colour figure can be viewed at wileyonlinelibrary.com]

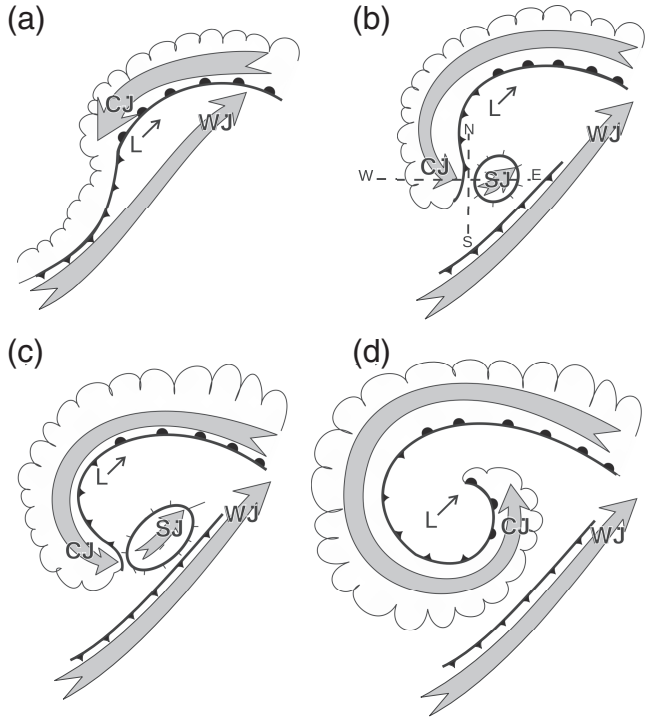

FIGURE 2 Conceptual model of the near-surface flows in an ETC. (a) Early stage of frontal wave cyclone development. L denotes low-pressure centre with direction of movement shown by the thin arrow. Grey arrows show the system-relative low-level jets; WJ is the warm-conveyor-belt jet (WCB in text) and CJ the cold conveyor- belt jet (CCB in text). (b) frontal-fracture phase, when the SJ first appears at the surface. (c) As the cloud head wraps round further, the SJ region extends. (d) Eventually the distinct SJ disappears and the dominant low-level wind in this region is due to the CJ. Positions of cross-sections shown in Figure 6 are marked in (b). Used with permission from Clark *et al.* (2005)

2011). The frontal fracture appears in stage II and persists in the mature system, stage IV. It is not present in the Norwegian model. Frontal fracture is defined by Browning and Roberts (1994) as "a major horizontal break or dislocation in the structure of a sharp cold-frontal transition occurring close to the centre of a developing cyclone." The proportion of cyclones that closely follow the SK life cycle, and so include a frontal-fracture stage, is not known.

The precise reason why some cyclones follow the SK evolution is not fully established. Some studies (as described by Schultz and Zhang, 2007) have argued that surface friction is important in determining which conceptual model a cyclone more closely follows. Other studies have argued that the large-scale environmental flow is important. As reviewed by Shapiro *et al.* (1999), many idealized model simulations have shown that cyclones developing within cyclonic barotropic shear (so-called Life Cycle 2: LC2) follow the Norwegian model whereas those developing without barotropic shear (Life Cycle 1: LC1) follow the SK model. In contrast, the studies of Schultz *et al.* (1998) and Schultz and Zhang (2007) examined the importance of along-jet, rather than across-jet, shear. They found that idealized cyclones (in a non-divergent barotropic model and a non-hydrostatic primitive equation model, respectively) entering a confluent background flow followed an evolution resembling the SK model (at least initially), whereas for a diffluent background flow the cyclones developed an occlusion resembling that of the Norwegian model. This finding suggests that SK-type cyclones may be more prevalent over the western North Atlantic Ocean (in the confluence region of the tropopause-level jet, e.g. Koch *et al.*, 2006), whereas Norwegian model-type cyclones may be more prevalent over the eastern North Atlantic Ocean and Western Europe. In other idealized simulations, cyclones initialized to the south of the axis of the tropopause-level jet developed following the SK evolution, whereas those initialized on the jet axis developed following the Norwegian conceptual model (Coronel *et al.*, 2016).

2.2 | The cloud head, dry intrusion and conveyor belts

The cloud that develops associated with the bent-back front in stage two of the SK evolution differs in structure from the occlusion of the Norwegian model, and has become known as the cloud head (Figure 2 shows a diagrammatic representation). It is often first visible as a "cloud leaf" emerging from under the polar front cloud band.

Böttger *et al.* (1975) first described the cloud head as a cirrus cloud configuration sharply separated from other clouds and characteristic of extratropical Atlantic storms that develop winds of hurricane intensity. Building on this, Bader *et al.* (1995) described a cloud head as existing when

TABLE 1 Criteria for instability: after Schultz and Schumacher (1999), simplified to remove some equivalents. ζ_z and ξ_z are the vertical components of absolute and relative vorticity (on pressure levels), respectively. See text for definitions of other symbols. Semicolon signifies that any of the conditions listed is sufficient

	Gravitational	Symmetric	Inertial
Dry	Absolute Instability $\frac{\partial\theta}{\partial z}<0$ $\left(\frac{\partial\theta_v}{\partial z}<0\right)$	Symmetric Instability $PV_g<0$; $\frac{\partial\theta}{\partial z}\Big\vert_{M_g}<0$; $\frac{\partial M_g}{\partial x}\Big\vert_{\theta}<0$	Inertial Instability $\zeta_z=\xi_z+f<0$
Conditional	Conditional Instability (CI) $\frac{\partial\theta_e^*}{\partial z}<0$	Conditional Symmetric Instability (CSI) $MPV_g^*<0$; $\frac{\partial\theta_e^*}{\partial z}\Big\vert_{M_g}<0$; $\frac{\partial M_g}{\partial x}\Big\vert_{\theta_e^*}<0$	N/A
Potential	Potential Instability (PI) $\frac{\partial\theta_e}{\partial z}<0$	Potential Symmetric Instability (PSI) $MPV_g<0$; $\frac{\partial\theta_e}{\partial z}\Big\vert_{M_g}<0$; $\frac{\partial M_g}{\partial x}\Big\vert_{\theta_e}<0$	N/A

an elongated area of layered cloud, lying poleward of the frontal cloud band, becomes broad (around 300 km wide), well-defined with a convex poleward edge and separated from the frontal band by a "prominent dry wedge" more commonly known as the dry slot. The cloud head is described as developing in the situation of almost zonal flow ahead of a flat, confluent upper-level trough due to a short-wave trough that triggers cyclogenesis.

The dry intrusion descends towards the cyclone centre from the upper troposphere (or occasionally lower stratosphere) and is associated with the dry slot region typically observed in satellite imagery. Intrusions of stratospheric origin correspond to tropopause folding in the vicinity of the upper-level jet stream. Dry intrusions can descend into the lower troposphere where destabilization beneath them can lead to enhanced near-surface wind gusts (Raveh-Rubin, 2017).

A cloud head and dry slot reflect aspects of the mesoscale structure of the flows within a cyclone. They are characteristic features of explosively deepening cyclones (central pressure falls exceeding 24 hPa in 24 hr at 60°N as defined by Sanders and Gyakum, 1980) which are also associated with exceptionally strong surface winds. Such strong surface winds also have a distinct mesoscale structure. They have been found in different parts of the cyclone in the form of elongated ribbons that have a lifetime in the system substantially longer than the time taken for a parcel of air to pass through them. Hence they have been dubbed "conveyor belts" (Browning and Roberts, 1994 give a set of definitions). Persistent strong surface winds are associated with the WCB on the warm side of the trailing cold front throughout much of the lifetime of an ETC (Browning, 1971; Harrold, 1973). The CCB on the cold side of the warm front often produces surface winds that are as strong or stronger as it wraps around the centre of the cyclone to become aligned with the system motion (Carlson, 1980; Schultz, 2001). It is thus shorter-lived than the WCB, but expected in the later stages of a storm's life cycle by forecasters.

The evolution of the relative strength of the cold and warm conveyor belts during cyclone development can be interpreted by analysing the redistribution of lower-tropospheric eddy kinetic energy. Rivière *et al.* (2015a; 2015b) investigate this redistribution in idealized and real extratropical cyclones, respectively (extending earlier work by Papritz and Schemm, 2013). They find that a low-level westerly jet develops to the south of the cyclone centre in the cyclonic shear case (when the cyclone is to the north of the baroclinic jet) due to the cyclonic redistribution of the energy by ageostrophic geopotential fluxes. The more intense low-level wind speeds are shown to evolve from the WCB region to the CCB region as a cyclone crosses the mean baroclinic jet location from the warm- to the cold-air side. Many cyclones undergoing explosive development have been found to cross the jet. For example, Pinto *et al.* (2009) found, using re-analysis data, that the core of the composite extreme cyclone during the maximum intensification stage had just crossed the 250 hPa jet. The cloud head was also noted as a signature of explosive cyclone development by Bader *et al.* (1995). This explosive development is described as accompanied by exceptionally strong winds in the region of cold advection at the tip of the CCB (Figure 2) which are attributed to rapid pressure rises behind the upper-level short-wave trough.

2.3 | Instabilities associated with extratropical cyclone structure

Much of the uncertainty surrounding the dynamics of SJs is related to the precise definitions and interpretations of various mesoscale instabilities that can occur within ETCs. These instability conditions are summarized in Table 1 and, as a practical example, Figure 3 illustrates in particular how Conditional Symmetric Instability (CSI), or neutrality to it, can occur at a cold front as well as Conditional Instability (CI). For the sake of clarity in the following sections, in this section we briefly review the relevant processes.

2.3.1 | Gravitational instability

Static instability refers to a local gravitational instability to infinitesimal amplitude fluctuations. In general, it may be assessed from $\partial b/\partial z$, where b is the buoyancy and z is height, taking into account any changes in buoyancy that arise through (infinitesimal) ascent or descent. In a cloud-free atmosphere, this is equivalent to $\partial\theta_v/\partial z$, where θ_v is the virtual potential temperature. Inside a cloud (assuming condensation occurs at 100% relative humidity (RH)) the buoyancy gradient is proportional to $\partial\theta_e/\partial z$ or, equivalently, $\partial\theta_w/\partial z$, (where θ_w and θ_e are wet-bulb and equivalent potential temperatures, respectively) plus a generally small term proportional to the vertical gradient of total water mixing ratio; a negative gradient indicates moist static instability. An

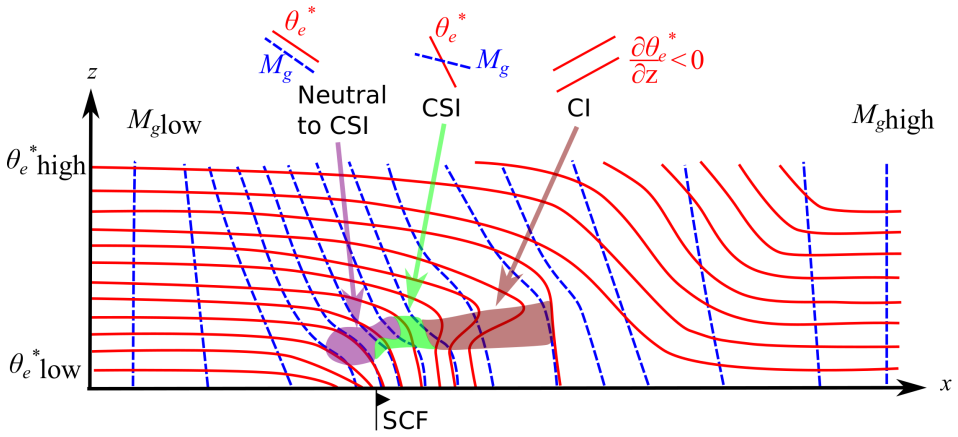

FIGURE 3 Diagram showing two-dimensional cross-section through a typical cold front. Saturated equivalent potential temperature (θ_e^*) surfaces are solid red, and geostrophic absolute momentum surfaces are dashed blue. The magenta region labelled "Neutral to CSI" is the region where M_g surfaces have the same gradient as θ_e^* surfaces. The green region labelled "CSI" is the region where M_g surfaces have a less steep gradient than θ_e^* surfaces. The brown region labelled "CI" is the region where θ_e^* decreases with height. Based on figure 4 of Schultz and Schumacher (1999) [Colour figure can be viewed at wileyonlinelibrary.com]

alternative way of describing static instability is in terms of the square of the appropriate buoyancy frequency, which must be negative for instability.

A linear stability analysis in cloud is based on there being sufficient condensed water to evaporate in the downward motion to maintain saturation. Once an instability starts growing, the environment of both upward and downward moving air becomes relevant, and the buoyancy of the downward moving air also depends on the continued supply of condensate to evaporate. This may be supplied either through the initial condensate in the air, or by precipitation falling into the air.

CI is a finite-amplitude (parcel) instability in that lifting a parcel (or, more strictly, adiabatic cooling by expansion associated with a pressure drop) by a finite amount, by some mechanism, is required to achieve saturation and hence generation of additional buoyancy by latent heat release by condensation. At this point, if further (infinitesimal) lifting results in the air having an environment with lower buoyancy, acceleration of the vertical motion occurs due to local instability.[1] Since θ_e and θ_w are conserved in adiabatic flow, comparison is often made between parcel θ_e or θ_w and the corresponding environment variable if the environment were saturated (θ_e^* or θ_w^*, the latter also being known as 'saturated wet-bulb potential temperature' or θ_s). Thus, assessment of the environmental static stability when saturated is made by computing the gradient of θ_e^* or θ_w^*, and the CI can be regarded as the (non-conservative) property of a point parcel. However, this is of no meaning when finite ascent is needed for saturation, and says nothing about the ultimate fate of such unstable parcels. In this case measures associated with finite parcel ascent are also commonly used, such as Convective Available Potential Energy (CAPE) and Convective INhibition (CIN)

Downdraughts often occur in convective clouds: they generally start off saturated and, so long as condensate is available, the stability and buoyancy considerations are much the same for as the rising saturated parcel. The gradient of θ_e^* or θ_w^* determines the local instability of the downdraught, while a "downdraught CAPE" or DCAPE, can be used to measure the finite displacement instability so long as the downdraught remains saturated.

Potential instability (PI), also known as "convective instability," is also a finite-amplitude instability, but referring to the lifting of a layer to saturation, so that not only θ_e and θ_w are conserved, but also their vertical gradients with respect to hydrostatic pressure (since the hydrostatic pressure-difference in the layer must also be conserved). Thus, if $\partial\theta_e/\partial z < 0$, the layer is potentially unstable, becoming moist statically unstable on lifting to saturation. In saturated air CI and PI are both equivalent to moist static instability.

In many numerical models, the cloud formation process is complicated by the assumption that, for large grid volumes, partial cloud can occur, so buoyancy can be generated by latent heat of condensation at mean RH<100%. For example, the MetUM uses the Smith (1990) cloud scheme, in which cloud (with increasing cloud fraction and liquid water content) forms as RH increases above a certain, specified, threshold, typically 80% in the free troposphere for global model configurations (higher values are used for convection-permitting configurations). Many mesoscale models that use a turbulence scheme based on the turbulent kinetic energy (TKE) use a similar idea but with a distribution of sub-grid cloud properties that depends upon the turbulence, based on ideas from Deardorff (1980). If such

[1]Though a very familiar concept, there seems to be no generally accepted term for buoyant instability in cloud, it often being simply labelled CI, even though the "condition" is, by definition, met. "Moist static instability" is also widely used. The current authors prefer "saturated static instability" as it is less ambiguous. The AMS glossary of meteorology first definition of CI leaves something to be desired. The definition refers to a "layer of unsaturated air" and "a parcel of air at the environmental temperature" being "unstable to upward vertical displacements if it is saturated," so it is clear that the layer is stable and must become saturated to become unstable. The main issue seems to be the process whereby it is assumed saturation takes place. If by lifting, then the definition is equivalent to potential instability. If by some other mechanism, the outcome depends on the precise mechanism considered.

a partial cloud scheme is used, the criteria for moist instability change as buoyancy production through condensation changes. In practice, these changes are often assumed to be small and hence ignored, not least because it is often (as in TKE-based schemes) impossible to state a general criterion, but the possibility of instability occurring close to, but at RH below, saturation should not be forgotten.

2.3.2 | Symmetric and inertial instability

Symmetric instability (SI) occurs when the Ertel potential vorticity (PV) is negative (Ooyama, 1966; Hoskins, 1974). SI is essentially a form of inertial instability (II) generalised to a baroclinic flow (and II is sometimes known as SI for this reason). However, it is important to note that the instability condition is essentially the condition for which the Sawyer–Eliassen equation in which the base-state PV is balanced is not elliptic (Sawyer, 1956; Eliassen, 1962).

The (semi-geostrophic) theory of symmetric instability is strictly two-dimensional and applied to a base state with a uniform thermal gradient, or frontal zone, in thermal wind balance. Thus, it is often discussed in terms of the geostrophic absolute momentum (also known as geostrophic pseudoangular momentum), defined by $M_g = v_g + fx$, with v_g the along-front geostrophic wind, f the Coriolis parameter and x is the cross-frontal direction. When $\partial M_g/\partial x < 0$ the flow is inertially unstable. This condition is equivalent to the geostrophic absolute vorticity being negative. Dry symmetric instability can be viewed as either dry gravitational instability on a M_g surface (i.e. $\partial\theta/\partial z|_{M_g}$) or inertial instability on an isentropic surface (i.e. $\partial M_g/\partial x|_\theta < 0$). Any slantwise displacement that occurs at an angle between the slopes of the M_g and θ surfaces will release the symmetric instability.

Analogous instability measures exist for slantwise convection and types of moist symmetric instability. Thus, CSI requires lifting to saturation, where the saturated equivalent geostrophic PV (denoted EPV^*_g or MPV^*_g where "E" is equivalent and "M" is moist) is the appropriate local instability measure (Bennetts and Hoskins, 1979). Since θ^*_e is not conserved in a parcel (except, of course, while that parcel is saturated), this local measure of CSI is only relevant in saturated air. θ_e is conserved in a parcel (saturated or not), so the (unsaturated) equivalent geostrophic potential vorticity (EPV_g or MPV_g) is a measure of instability, but it should, as noted by Schultz and Schumacher (1999), be regarded as a measure of "Potential Symmetric Instability" (PSI) because, by analogy with the dry case above, the criterion can also be expressed as $\partial\theta_e/\partial z|_{M_g}$ and hence relates to the vertical gradient of a layer lifted along M_g surfaces. As noted above, Figure 3 illustrates how surfaces of θ^*_e and M_g can be distorted at a cold front to produce regions with CSI or neutral to CSI, as well as regions with CI. Note that surfaces of θ^*_e are generally much more sloped than surfaces of θ, so CSI is more common than SI. Furthermore, air unstable with SI also possesses CSI, though, of course, SI does not require saturation to be released.

In saturated air, CSI and PSI are equivalent. Many authors use the full wind rather than the geostrophic wind to evaluate CSI (i.e. they use EPV^* or MPV^*). This choice is often due to the noisiness of calculated geostrophic winds in current operational-resolution weather forecast models, but can also be for theoretical reasons; these reasons are discussed in depth by Gray *et al.* (2011). Where finite ascent is required to achieve saturation, a parcel measure analogous to CAPE may be defined for slantwise ascent: slantwise CAPE or SCAPE (Emanuel, 1983), though care must be taken over the parcel path taken as, in practice, a system may develop significantly in the parcel-ascent time (Gray and Thorpe, 2001).

Slantwise downdraughts can occur analogously to vertical convective downdraughts. Clough and Franks (1991) show that sublimation of ice falling from cloud above can form a powerful mechanism for maintaining slantwise descent. Though Clough and Franks treat this as a distinct mechanism, it is not clear that this differs dynamically from CSI (apart from the latent heat of evaporation of ice rather than water, and total water is not conserved on a parcel). However, this does demonstrate that, provided the cloud above can maintain the supply of falling snow, saturation can be maintained over a shallow layer of a few hundred metres and hence maintain the instability of slantwise downdraughts. By analogy with DCAPE a "downdraught SCAPE" or DSCAPE can be defined (Gray *et al.*, 2011), though similar issues arise concerning the exact path to take the parcel in an evolving system as with SCAPE.

Static, conditional and potential instabilities can be released by flows that change the appropriate vertical gradients. Symmetric Instability (SI), at least as measured by the PV, has somewhat different properties. Since PV is conserved in a parcel in the absence of friction and diabatic processes, if a (point) parcel is unstable then it remains so until these processes act. It is not immediately obvious how the instability will ever be removed. Eventually, in a viscous fluid, viscous dissipation may be the ultimate instability release mechanism, but in practice in a numerical model, if the model's turbulence parametrization does not act first, slantwise motions will be produced that cannot be represented by the numerical scheme. In other words, numerical diffusion associated with the model dynamical core will destroy the instability. The same is true of CSI (or PSI) so long as saturation is maintained.

As stressed by Hoskins (1974), if a flow starts with positive PV (i.e. stable to SI), negative PV can only occur through the action of frictional effects and heat sources and sinks. In practice, while diabatic heating and cooling can readily change the PV, the manner in which negative PV can be generated warrants closer attention. The diabatic source term in the Ertel PV equation can be written

$$\frac{\boldsymbol{\zeta}}{\rho} \cdot \nabla\dot{\theta},$$

where $\boldsymbol{\zeta}$ is the absolute vorticity, ρ the density and $\dot{\theta}$ is the rate of change of θ on the parcel. Changes to PV by diabatic

processes primarily occur because of the resulting change in static stability (warming a layer reduces stability above and increases it below the layer). If there is time for the resulting flow to adjust to become balanced, then this change is communicated to the vorticity via the adjustment process. However, if the diabatic heating results in negative static stability, it is likely that local vertical mixing (reducing the stability and hence PV back to zero) will occur in a time much shorter than the adjustment time. Thus, it is highly unlikely that diabatic processes can produce long-lasting negative PV directly via production of negative static stability. However, changes to the direction of the θ gradient can, effectively, introduce vorticity into the PV component that was previously orthogonal to the θ gradient. In particular, horizontal gradients in diabatic heating can tilt θ surfaces away from horizontal and hence introduce *horizontal* vorticity into the PV. Thus, it is often helpful to consider the vorticity component (as well as the static stability) alongside the PV when considering diabatic heating.

Using the analysis of Haynes and McIntyre (1987), the PV follows the equation:

$$\sigma\frac{\mathrm{D}_\theta \mathrm{PV}}{\mathrm{D}t} = \mathrm{PV}\frac{\partial\sigma\dot{\theta}}{\partial\theta} - \nabla\cdot\left\{\dot{\theta}\frac{\partial v}{\partial\theta}, -\dot{\theta}\frac{\partial u}{\partial\theta}, 0\right\} - \nabla\cdot\mathbf{J_F}, \quad (1)$$

where σ is the mass density in isentropic coordinates, the material derivative denote material rate of change in isentropic coordinates, and the last term is the effect of friction, with $\mathbf{J_F} \equiv \{-F_y, F_x, 0\}$ and F_x and F_y the horizontal components of the frictional force. Since this equation uses θ as a vertical coordinate, $\dot{\theta}$ represents the movement of θ surfaces due to diabatic heating. The first term on the right is shown by Haynes and McIntyre to generally dominate and represents the "dilution" of PV by diabatic processes – as warming produces reduced or increased static stability, isentropic surfaces move apart or together. However, this term arises from the 3D flux of σPV, i.e. the 3D velocity $(u, v, \dot{\theta})$ multiplied by σPV, and cannot produce negative PV as it corresponds to a spatial redistribution of PV. Only the remaining two terms can do this, the first by bringing horizontal momentum into the isentropic layer in the presence of vertical shear, and hence horizontal vorticity.

2.4 | Multiple slantwise circulations

While frontal flows are generally considered as single, distinct entities, multiple slantwise circulations have been observed on a number of occasions. These are often inferred from the presence of multiple rainbands (Reuter and Yau, 1990) which are often associated with cold fronts, e.g. Fischer and Lalaurette (1995); Lemaître *et al.* (2001); Browning *et al.* (2001) They have also been observed in cloud heads, for example the cyclone observed during the Fronts and Atlantic Storm-Track EXperiment (FASTEX) intensive observing period 16 (Roberts and Forbes, 2002; Lean and Clark, 2003), where the circulations were strong enough to lead to the description of "multiple cloud heads." In some cases (such as this case from FASTEX), the downward branches of such circulations have been evident in the production of clear bands on the overlying cloud.

The presence of banded precipitation and hence banded ascent has often been associated with the presence and release of CSI though, as discussed by Schultz and Schumacher (1999); this association must be considered carefully and may have been spurious in some studies.

3 | DETECTION OF STING JETS IN OBSERVATIONS

3.1 | First identification

As discussed in section 1, B04 revisited the "Great Storm" of 16 October 1987. This was a particularly damaging example of a cyclone following the SK evolution. Having identified the surface SJ, he noted the development of (multiple) cloud bands with clear (or dark) bands in between infrared (IR) satellite imagery of the cloud head and in radar observations of surface rainfall. These cloud bands are shown in Figure 4, adapted from Browning and Field (2004). The cloud "tails" are identified with red lines, the clear or dark bands lying in between. He interpreted these clear bands as evidence that air was descending slantwise out of the cloud head into the frontal-fracture region, and showed a close

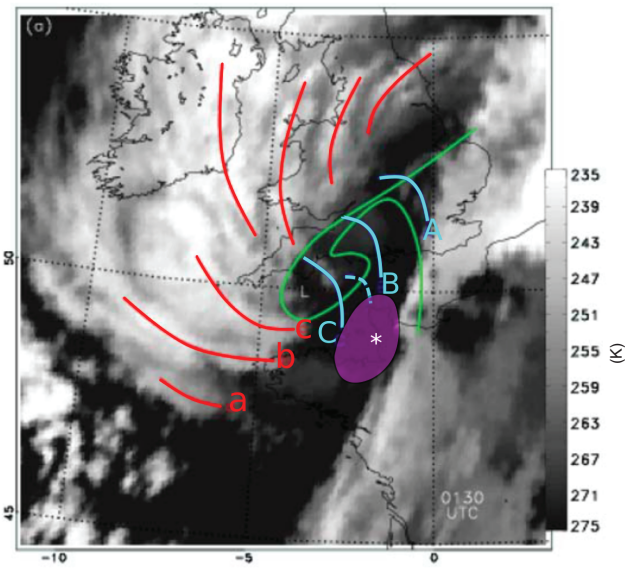

FIGURE 4 IR satellite images taken from the METEOSAT. Adapted from figure 3a of Browning and Field (2004). From the caption to the original figure: Axes of three cloud-head bands a, b, c (and four others) are denoted by red lines. The blue lines A, B and C, show the axes of boundary-layer convergence lines inferred from figure 4 of (Browning and Field, 2004). The dashed blue line shows one of the smaller "chevron" features discussed in the text. The green lines show the surface frontal analysis as explained in the text. L is the surface low-pressure centre and the small white asterisk denotes the centre of the region of strongest surface winds. The magenta oval has been added to show the strong gust region C in figure 9b of B04. Data courtesy EUMETSAT and Met Office

TABLE 2 Observed SJ windstorms. References given are to articles in which the presence of SJs in the named storms is explicitly discussed and demonstrated (other articles describing the impact and synoptic evolution of some of the storms also exist). Additionally, Hewson and Neu (2015) assessed that storms *Anatol* (3 December 1999), *Renate* (3 October 2006), *Xola* (23 December 2009), and *Petra* (15 July 2010) very probably (> 90% confidence) had SJs and that storms *Yuma* (24 December 1997), *Lothar* (26 December 1999), *Xynthia* (28 February 2010) and *Herta* (3 February 1990) probably (50–90% confidence) had SJs, although full analyses of the individual storms were not presented (their table 1)

Storm name	Storm date	Impact location	Reference
Great Storm	October 16, 1987	Southern England	Browning (2004); Browning and Field (2004); Clark *et al.* (2005); Gray *et al.* (2011)
Oratia	October 30, 2000	Wales and central England	Browning (2004); Browning (2005)
Anna	February 26, 2002	Central UK	Martínez-Alvarado *et al.* (2010); Gray *et al.* (2011)
Jeanette	October 27, 2002	Wales	Parton *et al.* (2009)
Gudrun/Erwin	January 7/8, 2005	Northern UK	Baker (2009); Gray *et al.* (2011)
Unnamed	December 7/8, 2005	East of Canada	Schultz and Sienkiewicz (2013)
Friedhelm	December 8, 2011	Scotland	Baker *et al.* (2013); Martínez-Alvarado *et al.* (2014a)
Ulli	January 3, 2012	Northern UK	Fox *et al.* (2012); Smart and Browning (2014)
St Jude's Day / *Christian*	October 28, 2013	Southern England	Browning *et al.* (2015)
Tini	February 12, 2014	Ireland, Wales, NW England	Slater *et al.* (2017);Volonté *et al.* (2018)

association between each clear band and enhanced gusts at the surface.

Browning and Field (2004) examined imagery from the storm in more detail and identified a series of very shallow arc-shaped and smaller chevron-shaped cloud features in the dry-slot region which were associated with damaging surface winds. They attribute these to boundary-layer convergence lines ahead of wind maxima associated with the downward transport of high momentum from multiple overrunning SJ flows (or, alternatively, multiple wind maxima within a single overall SJ) originating in the storm's main cloud head. Figure 4 shows the location of the strong surface gusts identified with the SJ in B04, the surface warm seclusion in the form of the surface frontal analysis and the boundary-layer convergence lines. The authors note that the southern parts of the surface convergence lines B and C were within, and tended to dissipate in, the low-θ_w flow that was encircling the warm seclusion, outside the southeast boundary of the warm seclusion and close to where the strongest surface gusts were recorded. The RH here tended to be in the range of 60–80%, compared to the near-saturation of the warm seclusion, indicating that this was a region where dry air was being mixed down.

3.2 | Other observed sting jet storms

Table 2 lists all of the storms in which SJs have been identified in detailed case-studies. Representative IR satellite images of the main western Atlantic storms are shown in Figure 5 (the one storm not included was too close to the edge of the satellite field of view for a sufficiently useful image). The images are (roughly) at the frontal fracture stage where the SJ would, by the B04 model, be reaching close to the surface. Note that, in many cases, the presence of a SJ was supported through model simulations (section 4); direct observation is difficult. One of the motivations for studying the Great Storm was that high-resolution paper anemographs were made (and had been archived due to the high impact of the storm). In many later UK cases (and climatological analysis indicates that North Atlantic SJ cyclones mainly impact the UK; Hart *et al.*, 2017), high-time-resolution surface data are not available; in the UK, as surface synoptic observations were increasingly being made using fully automatic weather stations, high-time-resolution measurements were no longer archived. Furthermore, for much of its existence, the SJ is above the surface and so other data sources are needed to identify a SJ. The situation regarding surface data is gradually improving over the UK and the recent study by Browning *et al.* (2015) made use of 1-min resolution surface data, as well as very-high-resolution Doppler radar data from the Chilbolton research radar.

Parton *et al.* (2009) used data from a VHF wind profiler at Aberystwyth, Wales, to make the first measurements of the vertical structure of a SJ with high spatial and temporal resolution in windstorm *Jeanette* (Wales, October 27, 2002). The VHF wind profiler measured mid–tropospheric winds (below 5 km altitude) at the tip of the cloud head, consistent with the SJ as defined above, and associated with vertical and horizontal banding (parallel to surfaces of θ_w); model output showed that the SJ was situated above a CCB jet (which was below the altitude observable by the radar). A UHF radar (situated further along the storm's track) measured strong winds attributed to the merger of the SJ and CCB. This article was the first to show that the SJ may lie entirely above the jet associated with the CCB and may be difficult to separate from it in the mature cyclone.

The first direct *in situ* measurements of a SJ were made during the field campaign of the DIAbatic influences on Mesoscale structures in ExTratropical storms (DIAMET) research project (Vaughan *et al.*, 2015). Windstorm *Friedhelm* (Scotland, 8 December 2011) was subject to intensive study as part of this project (Baker *et al.*, 2013; Martínez-Alvarado *et al.*, 2014a). These measurements (using dropsonde and *in situ* measurements) confirmed the separate identity of the SJ above the CCB, and also showed that model

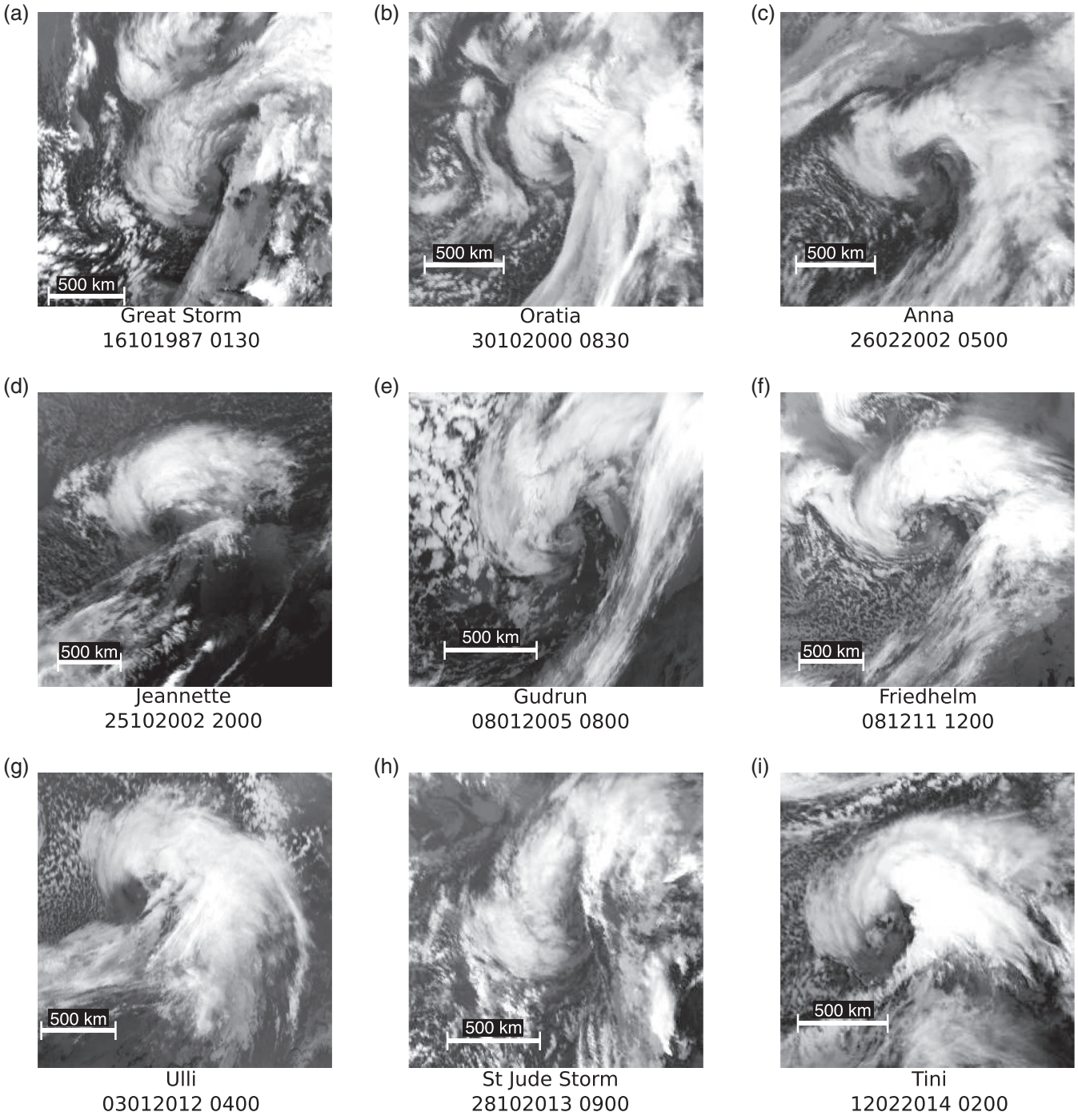

FIGURE 5 IR satellite images taken from the operational METEOSAT satellite at the time. Dates are given in dd mm yyyy format and times are UTC. Grey scale is arbitrary in each case and has been chosen to render the cloud features most clearly. Data courtesy EUMETSAT and Met Office

simulations captured the observed flow well. Whilst the *in situ* observations of windstorm *Friedhelm* are the first presented of a SJ, Martínez-Alvarado *et al.* (2014a) note that two previous experiments have made *in situ* observations from aircraft of the strong wind regions of ETCs, the March 8–10, 1987 storm (Shapiro and Keyser, 1990) and the storm observed during intensive observing period 4 of the ERICA experiment, the January 4–5, 1989 storm (Wakimoto *et al.*, 1992; Neiman *et al.*, 1993). These studies predate the "sting jet concept," and used dropwindsonde spacings considerably coarser than the approximately 30 km of the *Friedhelm* study; however, there are similarities in the observed structures. The 8–10 March 1987 case was observed with dropwindsonde and Doppler radar measurements in its T-bone phase (9 March) and fully secluded warm-core phase (10 March) and exhibits many of the features found in windstorm *Friedhelm*; however, the data are very likely to be too late in the storm's life cycle to show direct evidence of a SJ. The analyses of the January 4–5, 1989 storm certainly show the strongest low-level winds occurring in a similar region to the surface SJ location in B04 though, again, the data density is too sparse to identify any localized jet.

Hewson and Neu (2015) identified a number of storms as having SJs (with a range of confidence levels). These are listed in the caption of Table 2. The data used were primarily routine surface observations and satellite imagery. They define a SJ as "a small region affected by exceptionally high surface wind gusts, that occurred close to but downstream of the tip region of a cloud head of a cyclone that was undergoing, or had very recently undergone, rapid intensification."

However, a number of other more subtle criteria are also used. These are based on the characteristics of the SJ storms that have been studied in detail, together with hypotheses about their mechanism(s) of formation that are broadly consistent with the findings from detailed studies. Hence, it would be misleading to suggest that the storms identified by Hewson and Neu (2015) definitely contain SJs but they certainly confirm the existence of storms with characteristics *consistent with* the presence of a SJ.

3.3 | The association of sting jets with cloud-head bands

B04 proposed the presence of multiple clear bands, or equivalently of "filaments" or "fingers" of cloud at the tip of the cloud head (and hence multiple tails) as a "useful tool for nowcasting the occurrence and location of the worst winds."

The presence of multiple slantwise flows in cloud heads was supported by observations of multiple slantwise bands in the reflectivity signal from the Aberystwyth mesosphere–stratosphere–troposphere (MST) radar within storm *Oratia* on October 30, 2000 (B04, further analysed in Browning, 2005). Cloud bands and tails are clearly visible in IR satellite imagery (Figure 5b). The strong surface winds arising from the presumed SJ within this storm fortunately missed the UK.

Windstorm *Jeanette* exhibited this banded structure in IR satellite imagery (Figure 5d), rainfall radar and VHF wind profiler radar (Parton *et al.*, 2009). The SJ storm studied by Martínez-Alvarado *et al.* (2010) showed banding in IR satellite imagery (Figure 5c), though the cloud-head structure is a little unusual, possibly suggesting the presence of multiple cloud heads. Baker (2009) describe a SJ in windstorm *Gudrun*: imagery in this article shows a clear band in the cloud head (Figure 5e), but there is less evidence of multiple bands. Imagery of windstorm *Friedhelm* shows some evidence of a band in the cloud head (Baker *et al.*, 2013; Martínez-Alvarado *et al.*, 2014a and Figure 5f), though both satellite and radar imagery show multiple bands aligned approximately along the wind with approximately 50 km spacing, i.e. somewhat closer together than the more usual cloud-head bands. Smart and Browning (2014) studied the fine structure of a cloud head and its associated CCB and SJ in the intense ETC *Ulli*. This cyclone exhibited a very clear set of cloud bands and filaments at the tip of the cloud head (Figure 5g). Browning *et al.* (2015) studied the St Jude's Day storm. At the time the cyclone was over central England, satellite imagery showed two major cloud filaments (with a very distinct clear band between), but also some indication of a weaker clear band outside the outer filament. The radar rainfall rate very clearly shows several bands. Figure 5h) shows the storm a few hours later – two, and perhaps three dark bands are evident. Schultz and Sienkiewicz (2013) studied an ETC that deepened rapidly east of Canada during December 7–8, 2005. No satellite or radar imagery is shown in the article. Available geostationary imagery (GOES-12) and composites (Knapp *et al.*, 2011) suggest that at least one band was present in the cloud head, but the cyclone is located very far north and close to the edge of the region visible to the satellite. Windstorm *Tini* (Figure 5i), studied by Volonté *et al.* (2018), shows one of the clearest examples of multiple cloud-head bands and cloud tails.

Hewson and Neu (2015) use geostationary satellite imagery as a one of their main observational analysis tools and describe how the strongest surface gusts occur downwind of the gap regions between cloud filaments in the cloud-head tip region in several windstorms. However, since they use this as a primary criterion to identify SJ storms, this serves to confirm the association of cloud filaments with strong surface gusts in a location consistent with a SJ, but does not confirm the presence of a SJ.

From these studies it appears that SJs are associated with at least one clear band in the cloud head, and often with multiple bands. It must be remembered, though, that many of these studies used the presence of banding as an indicator that a SJ *may* be present in order to chose the cyclone for study in the first place; consequently, the presence of SJs in cyclones without these cloud-head signatures has not been systematically investigated. Nevertheless, the bulk of evidence seems to confirm Browning's suggestion that this cloud-head signature is, indeed, a useful nowcasting indicator and Fox *et al.* (2012) discuss its usage in their assessment of the Met Office forecasts, and their communication to the public, for windstorms *Friedhelm* and *Ulli*. The sample of cyclones analysed is relatively small, not least because the direct observation of a SJ is difficult and, in many cases, numerical modelling studies have been used to support the hypothesis that a SJ is present. There is no proven correspondence between banding and the existence of one or more SJs, but so far the observational link is quite strong. Reliance on model simulations to support the presence of a SJ has been necessary but cannot be regarded as satisfactory, especially as we do not know how robust simulations of SJs are.

3.4 | Summary of observational studies

Regions of strong mean winds and gusts have been observed at the surface in the frontal-fracture region of some severe cyclones following the SK life cycle. These are *distinct from* and *ahead of* the CCB. They are associated with a jet, termed a SJ, inferred to descend from the cloud head *above* the CCB. Direct observational evidence for these jets is fairly sparse, relying on a small number of wind-profiler observations and one *in situ* study. Single or multiple "clear" bands

in IR imagery appear to be strongly associated with these descending jets, though it has not been proven that *all* SJs are associated with such bands or *vice versa*.

4 | DETECTION OF STING JETS IN MODEL SIMULATIONS

As already discussed, it is very difficult to identify unequivocally a SJ from observations alone. While it may be possible to identify the SJ at or near the surface, it is often difficult to distinguish from the CCB in low-resolution observations; also its existence above the surface, in the cloud head, renders this part of its life very difficult to observe. The majority of studies of SJs have thus relied on analysis of model data to confirm the presence of the SJ.

4.1 | Characteristics of sting jets identified in model simulations

Clark *et al.* (2005) examined model simulations of the Great Storm in detail and confirmed Browning's interpretation of observations that the SJ (in this storm) is a distinct region of stronger winds that descends from mid-levels inside the cloud head into the frontal-fracture region of the cyclone over a period of a few hours. They summarized the structure of the simulated system using the conceptual diagrams reproduced in Figures 2 and 6. Figure 2 shows the location and timing of the surface manifestation of the SJ in the SK evolution, while Figure 6 shows cross-sections of the structure in the frontal-fracture phase. This emphasises that the SJ lay above the CCB during the early stage of its life and descended to reach the top of the boundary layer *ahead of* the CCB. The fact that it had higher θ_w (or equivalently θ_e) than the CCB and so was not on the cold side of the bent-back front is a very key characteristic of the SJ. The modelled SJ was quite short-lived at the surface (a few hours) and there may be several distinct pulses or jets, each associated with a descending band. These characteristics have been confirmed by a number of modelling studies of other cyclones (Baker, 2009; Parton *et al.*, 2009; Martínez-Alvarado *et al.*, 2010; Smart and Browning, 2014; Browning *et al.*, 2015) and model features have been confirmed by detailed observations (Baker *et al.*, 2013; Martínez-Alvarado *et al.*, 2014a).

Hewson and Neu (2015) suggest that no published model studies have shown the cloud-head bands and cloud filaments associated with SJs. There are very few illustrations of the paths of SJ trajectories in the literature and none show the relationship with cloud directly. However, there are many plots of time series of variables along SJ trajectories, and all show rapid reduction in RH to quite low values so clearly lead to dry regions within the cloud head. Since many studies now clearly show descending regions with associated reduction in RH, it is likely that this deficiency is more one of lack of explicit identification in the publication than actual

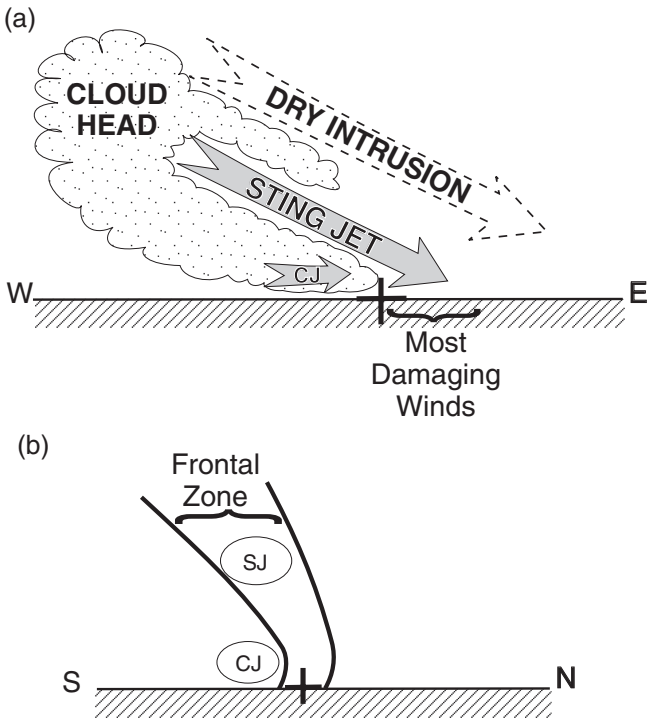

FIGURE 6 Conceptual model of cross-sections through the frontal-fracture region of an ETC (positions are shown in Figure 2b). (a) The west–east section shows the SJ descending from mid levels within the cloud head, beneath the descending dry intrusion and above CJ, the cold-conveyor-belt jet (CCB in text). (b) The south–north section shows the SJ as a distinct jet lying within the frontal zone separate from and above the CJ which lies close to the surface behind the frontal zone. Used with permission from Clark *et al.* (2005)

deficiency in the simulation. One reason why the concurrence of bands and SJ trajectories has not been illustrated is that the slantwise nature of the SJ motion and the bands makes it very difficult to plot in a plan view. For example, Clark *et al.* (2005) do show filaments at the tip of the cloud head, with the SJ descending between. There is a lack of distinct bands behind these filaments, probably an artefact of the smoothing of cloud produced by the sub-grid cloud model compounded by resolution, but the drier, descending layers are present in cross-sections.

While modelling studies support the existence of SJs, there is less evidence from modelling studies that multiple SJs can emerge from the cloud head. The Great Storm simulations of Clark *et al.* (2005) show multiple slantwise ascending layers, and suggest at least a second, weaker, descending SJ (their figures 6a and 16a). The COSMO simulations of storm *Anna* reported by Martínez-Alvarado *et al.* (2010) possibly show multiple SJs, but the MetUM simulations of the same cyclone do not. The St. Jude's Day storm simulations of Browning *et al.* (2015) suggest two SJs. The idealized simulations of Coronel *et al.* (2016) show a secondary dry band in addition to the major dry band associated with slantwise descent, though any associated enhancement in horizontal wind speed is weak.

It is possible that published results from models show less evidence of multiple SJs because, in general, their resolution

(especially vertical) is marginal for the simulation of such slantwise motions (section 4.3), but also because the authors have concentrated on the strongest SJ and simply not looked for more. Some support for the importance of model resolution for the representation of multiple rainbands comes from the convection-permitting (2.2 km grid spacing) ensemble results presented by Vaughan *et al.* (2015) for windstorm *Friedhelm*. Axes of 850 hPa wind speed maxima are shown to generally lie along the clear slots between rainbands in the cloud-head tip region in the each of the four sample ensemble members shown, although the precise location of the bands differs between members, as expected.

4.2 | The location of increase in horizontal speed of sting jets

It is very well understood that the CCB usually flows in a direction broadly opposite in direction to the system movement velocity over much of its path; thus, Earth-relative wind speeds can be quite weak. Only when it curves around to the southwest of the low (relative to the system movement direction in the Northern Hemisphere) does the CCB become aligned with the system velocity and hence Earth-relative winds become substantial. Thus, system-relative winds are needed to identify a contiguous conveyor belt. The same issue applies to the SJ. As a SJ curves around to the south of the system centre, its Earth-relative speed increases. The system-relative horizontal wind speed is a more interesting parameter. Here we review results for where this substantially increases along the path of SJs. Note that the term "acceleration" has often been used in the SJ literature with the danger of confusing speed increase with lateral acceleration in a curved flow.

In practice, the location and magnitude of SJ speed changes has not always been reported. Where it has, the situation is complicated by the fact that the system velocity may not be strictly constant, due both to the choice of coordinate system, and the fact that cyclones often slow down a little as the cloud head develops. We assume that this is a minor error, but needs to be considered as a *caveat*.

Many of the studies cited above use system-relative winds to help identify the SJ and CCB, but only Clark *et al.* (2005), Martínez-Alvarado *et al.* (2014a) and Volonté *et al.* (2018) actually report the history along SJ trajectories. Clark *et al.* (2005) shows some suggestion of an increase in system-relative wind speed in the SJ trajectories that descend the most (between 5 and 10 m/s), compared with the 25–30 m/s increase in Earth-relative speed. Martínez-Alvarado *et al.* (2014a) shows a more substantial increase in system-relative wind speed of up to 20 m/s. Volonté *et al.* (2018) shows an increase of about 15 m/s during the second half of the SJ descent.

In their study of a dry, idealized, cyclone, Slater *et al.* (2015) identify a "transitional" set of trajectories between the CCB and descending dry intrusion that descend into the wind speed maximum to the southwest of the system. Given the small number of trajectories described, it is not clear if these are actually part of a distinct jet, or just literally represent intermediate air; bearing in mind the continuum nature of the fluid, it is always possible to find a few back-trajectories which, if they arrive at points in between two distinct but connected regions, exhibit back-trajectory behaviour intermediate between these two regions. Assuming that they do represent a distinct jet, the authors show that some increase in speed can be associated with the along-wind pressure-gradient force encountered as they descend. The acceleration amounts to no more than about 2 m/s/hr, but acts over a very slow descent (over more than 12 hr); so these trajectories only loosely resemble SJs in observed systems. However, these simulations do serve to show that a weakly descending flow accelerates as it descends and encounters a stronger along-wind pressure gradient force. In contrast, the CCB in their system encounters a stronger along-wind pressure gradient force, but this is offset by surface friction.

Slater *et al.* (2017) show similarly descending and speeding-up trajectories (though with much faster descent rate), in a relatively low-resolution simulation (section 4.3) of cyclone *Tini* and confirm that the speed-up does, indeed, correspond to an along-wind pressure gradient. Other studies show the SJ as a distinct region of stronger system-relative wind speed at a given level, which suggests some system-relative increase in speed, but does not discount simple downward advection of stronger system-relative speed air.

The location of increase of kinetic energy of the air forming SJs provides some clues as to possible mechanisms for their formation. At present, this question can only be addressed using model studies, and not all published work has done so. Since friction usually acts against the flow, in most cases only the horizontal pressure gradient force ($\rho^{-1}\nabla_{\mathrm{h}}p$ where ρ is air density, p is pressure and the subscript h denotes that horizontal gradients are taken) can, of course, produce positive changes in horizontal kinetic energy, by whatever mechanism is operating. Furthermore, since the geostrophic component of the wind is perpendicular to the horizontal pressure gradient force, this force only does work on the ageostrophic component in the direction of the flow.

A complicating factor is the highly curved flow around the developing low pressure centre. For a very long time, forecasters have been taught to expect the strongest Earth-relative winds south of the centre of a developing low due to the superposition of the system velocity and system-relative cyclostrophic balance within the cyclone. In the simplest gradient-balance case (e.g. figure 3.5a in Holton, 2004) of a circular low-pressure region simply advected with a uniform Earth-relative flow, the system-relative wind is just a constant speed at a given radius from the centre of the low. The horizontal pressure gradient force due to the cyclone pressure field serves just to balance the Coriolis acceleration and the additional centripetal acceleration due to the circular motion around the low centre. It thus acts perpendicular

to the system-relative flow and does not contribute to any change in system-relative kinetic energy. The low-pressure region is then superimposed on the uniform pressure gradient balancing the uniform Earth-relative flow advecting the low-pressure system which therefore corresponds to the system velocity. Changes in Earth-relative kinetic energy actually come from the work done by the cyclone horizontal pressure gradient force on the uniform Earth-relative flow and the horizontal pressure gradient force associated with the uniform Earth-relative flow on the cyclone velocity. We expect a periodic variation in total Earth-relative kinetic energy of a parcel as it circulates the low, even in gradient wind balance in a moving system, with a minimum when the parcel is travelling against the system velocity (to the north of a west-to-east moving system) and a maximum when travelling with the system, to the south. This periodic variation in total Earth-relative kinetic energy is a real effect, of course, but says little about the dynamics of the system. Though such a simple, non-developing, barotropic system does not have distinct WCB and CCB, one can loosely associate the flow to the south of the west–east moving system with the WCB region and that to the north of the system with the CCB region. Rivière *et al.* (2015b) argue that, in real developing systems, the eddy kinetic energy redistribution from the WCB region to the CCB region as a cyclone crosses the mean baroclinic jet from the warm- to the cold-air side creates favourable synoptic conditions for SJs.

4.3 | Requirements for modelling sting jets

At the surface, the SJ observed by B04 was of order 50–100 km in horizontal scale. The spacing of cloud bands is typically about 100 km, so the descending region is around 50 km. Hewson and Neu (2015) also find that surface footprints of SJ damage are typically less than 100 km wide. While the precise number of grid points needed to represent a feature reasonably well depends upon the model, in general cases at least five or six points are needed, and preferably more (Lean and Clark, 2003; Skamarock *et al.*, 2014). It is not possible to give a precise criterion, as this depends upon the particular cyclone, the model, and the chosen quality criteria. However, it is therefore reasonable to expect that horizontal grid spacings of at most 10–15 km are required to model the phenomenon adequately. Smaller spacing than this may be needed to simulate the sub-structure of SJs, such as multiple descending pulses within the SJ, or interactions with the boundary layer, such as shallow convection, that may be needed to simulate resulting surface wind gusts. Hewson and Neu (2015) compared output from reanalyses and short-range forecasts at varying resolutions for windstorm *Ulli*, including the maximum gust speed in the SJ region, and found that grid spacing of less than about 20 km was needed for "satisfactory forecasts from a user perspective." They also suggest that higher resolution (10 km grid spacing or better) may be required to forecast very small cyclones such as *Lothar*, both from the point of view of the overall system intensity and features such as SJs.

Clark *et al.* (2005) suggested that a 12 km horizontal grid spacing requires a vertical grid spacing of about 240 m in the mid-troposphere. This follows the recommendations of Persson and Warner (1993) and the results of Lean and Clark (2003). Note that the constraint is motivated by the horizontal scale and slope of the flow (Persson and Warner, 1991), taken to be about one in fifty, and not by any assumed mechanism. However, the results of Forbes and Clark (2003) also suggest that this resolution is required to model the effect of the sublimation of snow below large-scale slantwise (frontal) ascents, and it should be noted that this is not just in order to capture the depth-scale of sublimation, but also to allow the consequently enhanced, and shallower, frontal descent to develop.

Note that it is the resolution, not the number of levels, that is important – some simulations include a greater overall depth of atmosphere than others and hence have lower resolution for the same number of levels. Furthermore, the important parameter is the vertical grid spacing in the mid-troposphere. Many operational forecast models now operate with 80 or more levels, but in many cases (e.g. the European Centre for Medium-range Weather forecasts (ECMWF) and Met Office global model) the additional levels are associated with much deeper modelled atmospheres and are included to improve stratospheric dynamics and satellite radiance data assimilation. These models still do not have the necessary vertical resolution to meet the criteria suggested above as needed to begin to represent SJs.

Table 3 summarizes the published information regarding resolution of simulations of SJ storms. All of the simulations listed appear to meet or come close to these criteria apart from those deliberately run to test sensitivity to resolution (italicized) and those marked in bold type. Clark *et al.* (2005) used 90 (non-uniformly spaced) vertical levels to achieve this resolution (200 m spacing at 5 km altitude, less below). The same model was also run using 38 levels (the standard operational at the time, 650 m spacing at 5 km altitude); the results were not reported in detail in the article because this resolution did, as expected, markedly degrade the model simulation, greatly reducing the modelled SJ strength *and its penetration towards the surface*. Martínez-Alvarado *et al.* (2010) tested sensitivity to vertical resolution in simulations using the MetUM with 12 km horizontal grid spacing and COSMO with 7 km horizontal grid spacing. They found that "both models produced storms of similar pressure depth to those performed with vertical resolution enhancements. However, the strongest winds (at 850 hPa) forecast by the former were restricted to significantly smaller areas than those forecast by the models with improved vertical resolution." Coronel *et al.* (2016) found that vertical level spacing of about 200–300 m in the mid-troposphere (2–5 km altitude) is needed to be able to distinguish a separate SJ and CCB jet in their idealized experiments. With this vertical resolution, they do not find

TABLE 3 Model resolutions used in SJ simulations. Entries in **bold** do not meet the minimum resolution requirements discussed in the text. Entries in italics do not meet the minimum resolution requirements for the release of mesoscale instabilities discussed in the text, but were run specifically to test sensitivity to resolution

		Horizontal grid	Vertical resolution	
Study	**Model**	**spacing (km)**	**Levels**	**Spacing**
Clark *et al.* (2005)	MetUM	12	90	200 m at 5 km
			38	650 m at 5 km
Parton *et al.* (2009)	MetUM	12	90	200 m at 5 km
Cao (2009)	MM4	**50**	**14 (300 hPa lid)**	**≈55 hPa at 800 hPa**
				≈70 hPa at 500 hPa
Martínez-Alvarado *et al.* (2010)	MetUM	12	76	200–370 m mid-troposphere
			38	*420–740* m
	COSMO	7	56	120–240 m mid-troposphere
			40	*230–400* m
Baker (2009); Gray *et al.* (2011); Baker *et al.* (2014)	MetUM	12	76	200–370 m mid-troposphere
Schultz and Sienkiewicz (2013)	WRF	12	Not specified	Not specified
Martínez-Alvarado *et al.* (2014a)	MetUM	12	70 (80 km lid)	170–275 m between 1 and 3 km
				275–350 m between 3 and 5 km
				(O. Martínez-Alvarado,
				personal communication, 2017)
Smart and Browning (2014); Browning *et al.* (2015)	WRF	5	48	120–240 m lower–mid-troposphere
Slater *et al.* (2015)	WRF (dry)	10	*40*	Not specified
		20	*40*	Not specified
		10	80	Not specified
		20	80	Not specified
Coronel *et al.* (2016)	Meso-NH	4	Not specified	200–300 m at 2–5 km
		20		200–300 m at 2–5 km
		20		*500* m
Slater *et al.* (2017)	WRF	**20**	39 (≈50 hPa lid)	8 of below 850 hPa
Volonté *et al.* (2018)	MetUM	12	70 (40 km lid)	120–200 m between 1 and 3 km
		24		200–260 m between 3 and 5 km
			70 (80 km lid)	170–300 m between 1 and 3 km
				275–350 m between 3 and 5 km

very much sensitivity to horizontal resolution, finding similar results with 20 and 4 km horizontal grid spacing. However, the jets were not distinguishable with coarser vertical resolution, while enhanced (80 m) vertical level spacing (with 4 km horizontal grid spacing) did not substantially change the results. In contrast, Slater *et al.* (2015) found little sensitivity to resolution in their idealized simulations, though it may be relevant that their study is of a *dry* cyclone (so no changes in PV can occur due to moist processes).

In some studies only the number of vertical levels has been stated without further information on the levels used. Martínez-Alvarado *et al.* (2014a) used 70 levels, but with an 80 km lid. They do not state the vertical resolution but the operational Met Office global configuration was used, and this information has been added to the table (O. Martínez-Alvarado, personal communication, 2017). This configuration gives similar mid-troposphere spacing to the 76 levels used with a 40 km lid by other authors using the MetUM, and the 12 km simulations verify remarkably well. Slater *et al.* (2017) utilized a model top at 50 hPa and 39 vertical levels, eight of those below 850 hPa in their configuration of WRF with 20 km horizontal grid. Volonté *et al.* (2018) studied the same storm using a MetUM configuration meeting the suggested criteria and one that did not (i.e. 24 km horizontal resolution, 300 m spacing at 3 km – the same levels as used by Martínez-Alvarado *et al.* (2014a)). Results confirmed that the nature of the solution at lower resolution was similar to that of Slater *et al.* (2017) but was qualitatively different at the higher resolution, suggesting that, in this case, horizontal resolution was a more controlling factor than vertical. Finally, Cao (2009) is included in this table as the authors attribute to a SJ the strong surface winds at the tip of the bent-back front and cloud head in an idealized cyclone. However, no evidence is presented that these result from a jet descending from the cloud head and it is highly likely that they are part of the CCB, though it is difficult to be precise given the low resolution of

the model (50 km horizontal grid spacing with only 14 model levels).

The resolution limitations discussed above are only estimates, but it must be remembered that they represent the minimum required to start to represent the phenomenon adequately. Most of the studies discussed are just meeting these minimum requirements, and there is undoubtedly a need for much better resolved simulations, especially in the vertical. Furthermore, these restrictions imply, for example, that the descending airstreams diagnosed in the articles by Slater *et al.* (2015; 2017) (both 20 km horizontal grid spacing, but with 39 and 40 vertical levels, respectively) are unlikely to be fully developed SJs, if they are SJs at all. This is discussed further below.

A further indication of the importance of horizontal resolution comes from the comparison of the time evolution of CSI release in the SJ in different resolution models. Gray *et al.* (2011) conclude that the release of CSI (inferred from reduction of the fraction of points in the cloud head that are unstable to CSI with time) in the SJ air is substantially delayed in a forecast with ≈45 km horizontal grid spacing compared to a forecast with 12 km grid spacing. This implies that the coarser resolution model is less able to release CSI and so less able to represent SJs if this process is important for their generation and/or maintenance.

SJs have been found in a number of different models, and so do not appear to be an artefact of the formulation of a particular model. However, little is known about the robustness of simulations, in particular whether different models would produce similar solutions. The only multi-model study of a SJ is that reported by Martínez-Alvarado *et al.* (2010); this shows very similar structure of the SJ in the models, but with different timing. It should be emphasized, however, that the two models used (COSMO and MetUM) each started from the same ECMWF global analysis, but both showed some sensitivity to the choice of initial conditions. This said, the study seems to support the hypothesis that the presence and broad structure of a SJ is consistent between models, but the detailed structure and timing is not.

4.4 | Summary of modelling results and definition of sting jets

The observational and modelling studies discussed above have shown that a significant number of cyclones have features that support the conceptual model of the morphology of a SJ proposed by Clark *et al.* (2005) and illustrated in Figures 2 and 6. This is further illustrated in the three-dimensional representation in Figure 7, which shows the relationship between the SJ, CCB and WCB in a cyclone with SK evolution.

The SJ is defined as a coherent air flow that descends from mid-levels inside the cloud head into the frontal-fracture region of a SK cyclone over a period of a few hours leading to a distinct region of near-surface stronger winds. It therefore lies above the CCB during some stage its life, but, at least in some cases, descends to reach the top of the boundary layer ahead of the CCB. It is not attributed to a specific mechanism in this definition. This definition of a SJ has evolved from the modelling study of Clark *et al.* (2005). Strong near-surface wind speeds and gusts may or may not result from a SJ depending on boundary layer processes. This definition differs slightly from that in B04 derived from surface wind observations: he states, in relation to low-level winds, "We refer to this dry-slot wind maximum as the sting at the end of the tail." So, he instead defines what has come to be known as the SJ as the resultant near-surface winds of the SJ as defined here.

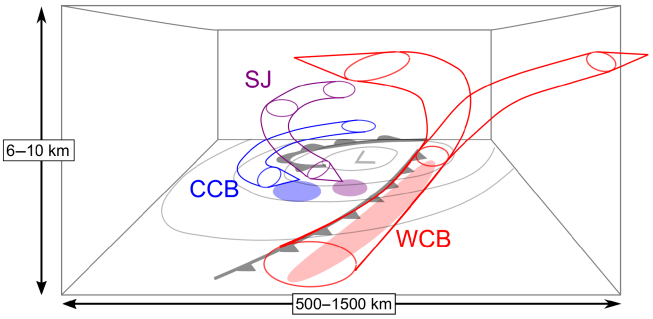

FIGURE 7 Conceptual model of the 3D structure of a SK cyclone showing the WCB (red), CCB (blue) and SJ (magenta). In each case the region of strong surface winds is indicated by an ellipse [Colour figure can be viewed at wileyonlinelibrary.com]

5 | MECHANISMS FOR STING JET FORMATION

The precise mechanism (or mechanisms) responsible for the SJ is/are yet to be fully understood. Given the definition in section 4.4, we need to understand why such a distinct region of strong winds occurs, what determines its strength and spatial scale, why the air descends from mid-levels within the cloud head and what determines its rate of descent and timing. Furthermore, a complete mechanism needs to explain why, in some cases at least, multiple SJs may occur.

5.1 | First ideas

As explained in section 4.2, even a perfectly balanced steady moving cyclone would be expected to have stronger Earth-relative winds on the southern side of the low centre. B04 recognised that the gradient wind was "sufficient to account for a large part of the strength of the surface winds in terms of balanced dynamics." He also recognised that the SJ occurs in a region of general descent out of the cloud head into the frontal-fracture region. (e.g. the analyses of cloud-head flows in figure 5 of Browning *et al.*, 1995, or figure 8 of Browning and Roberts, 1994), though he did not explicitly identify frontal fracture with frontolysis. However, he hypothesised that the jet may be *enhanced* by evaporation in the

strongly descending parts of slantwise circulations within the cloud head. This may happen where precipitation falls into the descending flow from the overlying ascending flow, but there may also be significant condensate to evaporate at the start of descent. In addition, he suggested that the multiple slantwise circulations may be evidence of the release of CSI associated with diabatically generated negative EPV_g^* (or MPV_g^*) as had been observed in other explosively developing cyclones. He also hypothesised that the resulting reduction in static stability may have enhanced momentum transport to the surface.

The identification of strong SJs with the release of CSI developed within the cloud head was clearly based upon Browning's hypothesis that release of instability may *enhance* the strong winds arising from the balanced dynamics taking place within the cloud head, especially the frontal-fracture region. Although this enhancement may be small in relative terms (e.g. B04 considered an increase from 45 to 50 m/s for the Great Storm), this can cause a large increase in damage because damage is typically considered to depend on wind speed cubed above a threshold (e.g. as used by Leckebusch *et al.*, 2008, in the justification for their storm severity index).

Figure 14 of B04 shows a schematic of multiple slantwise circulations, including cross-sections transverse to the bent-back front in the cloud head, with the implication that the primary enhancement in the flow due to these circulations is in the transverse direction. The air emerging from the tip of the cloud head is taken to be dominated by the descending branches of these slantwise circulations. It is not evident from the article why the speed in the along-front direction is markedly changed, though there is a clear implication in both B04 and Browning and Field (2004) that the SJ accelerates to be ahead of the CCB, and hence in the along-front direction. It should also be remembered that in the frontal fracture region there is no strong frontal zone and the orientation of the temperature gradient is changing rapidly relative to the flow. Furthermore, while less effective in increasing the overall kinetic energy than a speed change in the along-front direction, an enhancement in the speed in the transverse direction (and hence, overall, a change in direction of the flow) is sufficient to increase the overall speed and hence damage potential of the jet.

5.2 | The role of large-scale cyclone dynamics

Schultz and Sienkiewicz (2013), in a case-study, explicitly demonstrated that an airstream descending out of the studied cloud head is associated with frontolysis which, in turn, is associated with the frontal-fracture region. This seems consistent with Browning's view that balanced dynamics is sufficient to account for much of the surface wind and also with the attribution of strong winds near the tip of the cloud-head hook to a rapid surface pressure rise by Bader *et al.* (1995). Similarly, Coronel *et al.* (2016) show that the descent of air ahead of the bent-back warm front region of their idealized cyclones occurs in a region where the **Q** vector (Hoskins *et al.*, 1978) is divergent, implicating geostrophic forcing in the descent. In Coronel *et al.* (2016), the divergence of the **Q** vector is shown to be dominated by its along-front component rather than its cross-frontal component, which the authors state suggests that the frontolytic mechanism of Schultz and Sienkiewicz (2013) does not entirely explain the geostrophic forcing of the descent. However, we note that the **Q** vector orientations and associated divergence patterns in figure 13a of Coronel *et al.* (2016) could arise in a situation of combined deformation frontolysis (dominating near the end of the bent-back front) and shear frontogenesis (dominating further back along the front in the **Q** vector convergence region) for example.

Slater *et al.* (2017) also attribute the strong surface winds to the southwest of the centre of windstorm *Tini* to the large-scale dynamics of the cyclone (inferred from analysis of the terms in the horizontal momentum equation and the diagnosis of the quasi-geostrophic omega and **Q** vectors). Unlike higher-resolution case-study analyses (e.g. figure 4a,b of Martínez-Alvarado *et al.*, 2014a, and figure 6c of Baker *et al.*, 2014), the feature identified as a SJ does not form a vertically distinct wind maximum at low levels, instead appearing as a lower-level extension of the upper-tropospheric jet. It must be borne in mind that the resolution used in the Slater *et al.* (2017) study (20 km grid spacing and 39 vertical levels) excludes the possibility that CSI or SI could be released. Nevertheless, the simulated wind speed is strong (45–48 m/s), does (according to the small sample of trajectories followed) descend out of the cloud head, and is ahead of, and distinct from, the CCB.

As discussed in section 4.2, a number of authors have related the increase in SJ winds to the horizontal along-wind (and hence ageostrophic) pressure gradient. Since this must be true of all mechanisms, it adds little to our understanding, but it does draw attention back to the pressure field. As discussed above, gradient wind balance in a moving system accounts for some, and possibly much, of the strong winds on the southern flank of the cyclone. Slater *et al.* (2015; 2017) further demonstrate the role of frontolytic descent into the frontal-fracture region as bringing air down into a region of larger pressure gradient nearer the surface. The horizontal pressure gradient force is often largest to the southwest of developing SK cyclones (section 4.2).

Thus the downwards advection of strong winds from aloft due to the frontolytical secondary circulation, and further acceleration by the low-level pressure gradient may well describe the role of large-scale cyclone (semi-geostrophic) dynamics in setting the scene and can, in some systems, produce strong winds with characteristics ascribed to SJs. However, these results do not rule out the possibility of further enhancement of the wind in some cases, as indeed was recognised by Schultz and Sienkiewicz (2013). Such enhancement would be important in itself, but it would also increase the likelihood that the jet descends further ahead of the CCB and may produce strong surface winds ahead of the CCB.

These results neither preclude nor prove the possibility of CSI or SI release in some systems. Furthermore, they do not explain observations of multiple descending branches in some systems.

5.3 | The role of CSI release

There are many questions regarding the precise mechanism through which CSI release may contribute to SJ generation and/or maintenance. As pointed out in depth by Schultz and Schumacher (1999), some care needs to be taken in defining and using concepts related to CSI and moist instability in general. Caveats such as two-dimensionality of the flow (in the case of CSI and SI) are difficult to manage in the absence of a more complete three-dimensional theory. Issues surrounding the saturation of the air being considered are more straightforward.

B04 clearly took it for granted that the air in the cloud head, at least before descent of the SJ, has undergone some ascent and is saturated. Furthermore, the air is cloudy so at least some condensate is present to maintain saturation during initial descent. However, the descending SJ will eventually become unsaturated unless there is sufficient initial condensate or a supply of condensate from elsewhere to maintain saturation. This consideration is thus related to Browning's suggestion that evaporating precipitation may play a role.

Gray *et al.* (2011) examined a number of instability diagnostics in simulations of four severe storms. Three of these storms exhibited a SJ and one of them did not by their criteria for a SJ (especially wind strength) even though it had many of the apparent features of SJ storms and did show a *weakly* descending airflow out of the cloud head (presumably attributable to frontolysis). In the SJ storms, they concluded that CSI "released by descending air parcels, as diagnosed by decaying DSCAPE, is collocated with the SJs in all three SJ storms and has a localized maximum in two of them." They thus "conclude that CSI release has a role in the generation of the SJ, that the SJ may be driven by the release of instability to both ascending and descending parcels, and that DSCAPE could be used as a discriminating diagnostic for the SJ." A similar pattern of decrease in CSI was reported in model simulations of windstorm *Friedhelm* by Martínez-Alvarado *et al.* (2014a).

The resolution requirements discussed in section 4.3 are based on observed scales of SJs, but are similar to those required for CSI and SI (Ducrocq, 1993). The results of Slater *et al.* (2017) in section 5.2 appear to contradict these requirements and therefore can shed no light on the role of CSI or SI. Model simulations that cannot simulate the mesoscale instabilities in question cannot demonstrate that they do not occur. However, they do show a strong-wind feature which meets the definition of a SJ, which suggests that CSI or SI are not *necessary* for a SJ to occur. This contradiction is resolved by recent simulations of the same storm (*Tini*) using the MetUM (Volonté *et al.*, 2018). Lower-resolution simulations reproduce the results of Slater *et al.* (2017). However, higher-resolution simulations meeting the criteria in section 4.3 show that an additional mechanism associated with generation and release of CSI/SI produces a much stronger and more distinct jet, enhancing the speed from 45–48 to 60 $\mathrm{m\,s^{-1}}$.

Smart and Browning (2014) find no evidence that CSI release had a "major role" in the development of SJs in windstorm *Ulli*. However, their diagnosis was based on the evolution of *MPV* calculated using the unsaturated, rather than saturated, θ_e and hence was a diagnosis for PSI rather than CSI (D. J. Smart, personal communication, 2017). This calculation may yield slightly different results regarding CSI if partial saturation is assumed to exist at <100% RH (which can be a reasonable assumption for numerical model output (section 2.3), and has been assumed when inferring CSI in e.g. Martínez-Alvarado *et al.*, 2014a). Indeed, Hart *et al.* (2017) (discussed further below) state that windstorm *Ulli* showed the presence of a weak CSI diagnostic (in ERA-I data) that was insufficient to meet their criteria. It is therefore possible that the role of CSI has been underestimated in this article. Nevertheless, this case provides some evidence in support of the hypothesis that a flow meeting the definition of an SJ can occur in a cyclone that is not strongly unstable to CSI.

The majority of strong SJs studied using model simulations have originated in regions with MPV^* close to zero or negative. Some controversy in the literature may arise from the use of relatively arbitrary thresholds to interpret the strength of SJs and MPV^* signatures. For example, Coronel *et al.* (2016) show the presence of negative MPV^* regions in vertical cross-sections through the frontal zone of their idealized cyclones. The spatial scale of these regions is certainly consistent with the scale of SJs. However, they consider that the spatially localized nature of these negative MPV^* regions together with near-zero (negative for a few hours) values of MPV^* along the majority of back-trajectories initialized in the low-level SJ correspond to near-neutral environment with respect to CSI. An alternative interpretation is that these are signatures that CSI has been (or is continuously being) released.

5.4 | The role of SI and II release

Discussion of CSI is contingent on the assumption that the air being considered is saturated and has some condensate to evaporate, as is generally the case with air in the cloud head at the origin of SJs. However some model studies (e.g. Clark *et al.*, 2005) have shown regions of negative PV in the region of the SJ origin in the cloud head as well as negative *EPV*, in which case consideration of moisture and saturation is less relevant (since *EPV* is equal to EPV^* in a saturated environment).

Other work has diagnosed inertial instability in the SJ and inferred that its release may also accelerate SJs. In general, given the likelihood that the environment is not strictly

barotropic, this might best be interpreted as showing SI, but in most cases the II was diagnosed purely from the vorticity. The idealized model study of Baker *et al.* (2014) diagnosed SJ trajectories as inertially unstable in their simulation with the weakest initial static stability. Buckled absolute momentum surfaces, implying II, were generated in the idealized simulation of Coronel *et al.* (2016) with high vertical and horizontal resolution. Inertial instability was also diagnosed as existing in narrow bands wrapping round within the modelled cloud head of windstorm *Friedhelm* and shown to be present in the descending SJ airstream (Martínez-Alvarado *et al.*, 2014a).

Unfortunately, the release of slantwise instabilities can lead to extremely distorted flows in which other instabilities may be diagnosed. As discussed in the *Friedhelm* study above, the release of CSI can lead to the buckling of absolute momentum surfaces, and hence the diagnosis of II (as negative vertical component of absolute vorticity). Similar buckling, observed in a lower frontal zone using high-resolution dropsonde data, has been described by Thorpe and Clough (1991) as resulting from, and, indeed, "direct evidence of ", CSI release. Notably the presence of near neutrality to CSI (inferred from parallel absolute momentum and θ_e^* surfaces) in the mid- and upper-frontal zone is considered to probably be a consequence of CSI release. This mechanism is analogous to Delta-M adjustment, the term given to the momentum surface buckling that can result from CI release in cold frontal zones leading to frontal rainbands (Holt and Thorpe, 1991; Pizzamei *et al.*, 2005; Morcrette and Browning, 2006).

For the most part, an association between CSI and SI and the enhancement of horizontal wind speed has been been based upon energetics – the observation (in model simulations) that before descent an unstable air parcel has DSCAPE, while at the bottom of its descent the parcel is no longer unstable and has more kinetic energy. Conversely, low-resolution simulations that develop the DSCAPE but do not release it have lower kinetic energy in any descending flows that do occur. As discussed in section 5.1, it is not clear how slantwise descent in the radial direction of the cyclone, i.e. transverse to the bent-back front, can lead to along-flow speed-up. As suggested, this may not be crucial anyway, as transverse acceleration can also contribute to the overall speed, but some indication that increase in speed along the flow may occur is provided by Jones and Thorpe (1992) who studied some three-dimensional aspects of SI and CSI. They considered a number of scenarios that add three-dimensionality to the classic SI analysis. Though it is difficult to associate directly these scenarios with the SJ environment as any or all of them may apply, a common result was a modest increase in the along-front wind speed in the descending branches of SI/CSI circulations. In their case, only about 2 m/s speed-up occurred, but their scenarios had relatively modest instability and growth rates compared with those observed in strong SJs, so a speed-up of 5 m/s or more seems plausible. Note that, while their study was three-dimensional, the base state was still a straight frontal zone, so the role of curvature remains unknown.

5.5 | The role of frontal dynamics

As described in the previous subsections, there is thus a body of evidence in support of the hypothesis that mesoscale instabilities enhance the descending and accelerating flow in the SJ. There is also evidence that the SJ occurs in a region of descent due to frontolysis and that, at least in some extreme cases, this descent into a region of strong low-level horizontal pressure gradient is sufficient to produce strong winds in a mesoscale jet. It is thus reasonable to ask what role frontal dynamics has in the development of SJs.

However, it is very difficult to separate the effects of frontal dynamics from such mesoscale instabilities, as fronts often occur in regions with weak slantwise convective stability (as summarized by Schultz and Schumacher, 1999). In dry frontogenesis, as discussed through the Sawyer–Eliassen equation, the symmetric stability modulates the response to forcing. Analogous impacts occur in cloud, complicated by the asymmetry of saturated updraughts and unsaturated downdraughts.

In particular, Emanuel (1985) discusses the impact of small stability to slantwise convection on frontogenesis. Thorpe and Emanuel (1985) discuss this further in the context of diabatic heating by condensation in the frontal ascent. They show that "in an atmosphere which has small stability to slantwise convection, frontogenesis proceeds at a much increased rate and the horizontal scale of the ascent in the warm air is considerably reduced. One main conclusion, therefore, is that cross-frontal circulations produced by geostrophic forcing are similar in structure to slantwise convection, despite (small) stability to the latter."

Similar conclusions seem to apply to frontal descent on the cold side of the front where evaporation of rain (Huang and Emanuel, 1991) or sublimation of ice (Forbes and Clark, 2003) occurs. The latent cooling leads to the production of a strong, shallow, sloping downdraught. Xu (1989) went further by solving an extended moist Sawyer–Eliassen equation including the effects of eddy viscosity and small instability to slantwise convection under weak frontal forcing conditions. Multiple bands resulted, with sufficiently negative stability and widespread forcing (relative to the semi-geostrophic Rossby radius of deformation), which had similar characteristics to observed rainbands. Thus, where saturation is maintained and stability is small with respect to slantwise convection, it appears that frontal descents produced by geostrophic forcing are also similar in structure to slantwise convection, having a strong jet confined to a very shallow vertical scale.

5.6 | The role of evaporative cooling

Since descent starts within the cloud head, some condensate will be present in air as it starts to descend. This may be

replenished by precipitation falling from above to produce latent cooling (as in the frontal descent studied by Forbes and Clark, 2003). As discussed in section 2.3.2, it is not clear that the dynamics differ from usual considerations of frontal and CSI dynamics apart from the identification of a source (precipitation from cloud above the descending layer) to maintain saturation. Nevertheless, since the maintenance of saturation does depend on the presence of precipitation, it has often been discussed as a separate mechanism (in much the same way as the role of stratiform precipitation in the dynamics of mesoscale convective systems has been discussed). Evaporative cooling may also affect the transfer of high momentum from the top of the boundary layer towards the surface; this is considered in section 6.

Baker *et al.* (2014) show that turning off evaporation effects in idealized simulations led to no significant change to the wind strength or descent rate of the SJ. Coronel *et al.* (2016) found only a slight (2 m/s) decrease in low-level horizontal wind speed when they performed a similar experiment, even though there were strong indications that three of the nine back-trajectories they analysed underwent evaporative cooling. Thus, while evaporative cooling may be occurring, it seems unlikely that this additional latent cooling is *essential* for the formation of a SJ.

However, the evaporative cooling in these idealized cases was only one or two degrees. Smart and Browning (2014) similarly diagnosed cooling of generally less than a degree in the SJ of windstorm *Ulli*. It is notable that the descending airstream in Slater *et al.* (2017) accelerates markedly during descent. The authors diagnose the cooling in potential temperature that occurs during descent to be up to 4 K prior to entering the boundary layer. They refer to this as "little change," and conclude that evaporative effects (referred to as "warming" whereas it is likely that "cooling" was meant) are not important in the descent. In contrast, Clark *et al.* (2005) showed that there was a strong correlation between descent and potential cooling in the SJ of the Great Storm. While there was potential cooling of only 0.7 ± 0.1 K averaged over the entire population of trajectories considered to be part of the SJ (many of which had warmed at low levels), those trajectories that descended most cooled typically in the range 3–8 K (while maintaining approximately constant θ_w). The buoyancy represented by 4 K cooling if air descended through 3 km would represent the release of available potential energy of around 400 J kg^{-1}. This is not huge, but it is clearly not negligible (it would represent an increase in wind speed from 40 to nearly 49 m/s if all converted to kinetic energy). It remains plausible that such strong cooling may have modified the flow in both of the above cases.

Finally, it is notable that the idealized set-ups of both Baker *et al.* (2014) and Coronel *et al.* (2016) were of cyclones cooler and drier than those typically observed; Baker *et al.* (2014) used an initial RH of 80%, but a surface temperature that was near freezing at 55°N, and Coronel *et al.* (2016) used an initial lower-tropospheric RH of 60% and similarly low temperatures. Baker *et al.* (2014) commented that their low temperatures would likely have resulted in reduced cloud formation compared to typical observed SJ cyclones; consequently the role of moist diabatic processes in these idealized SJs may be less than that in real cases.

5.7 | Summary of mechanisms for sting jet formation

Considering the discussion above, it seems likely that a continuum of behaviour occurs, from balanced descent partly associated with frontolysis in the frontal-fracture region, through horizontally smaller scale and stronger frontolytic descent associated with weak stability to slantwise convective downdraughts, to multiple slantwise convective downdraughts associated with the release of CSI and even, possibly, SI. This descent brings air which already has a relatively high speed from mid-levels towards the surface, but further increase in speed occurs during descent. Quasi-geostrophic frontolytic descent alone can produce substantial speed-up as air reaches lower levels with larger along-flow pressure gradient. Significant additional speed-up has been demonstrated to be associated with the release of CSI and SI, though it is very difficult to separate the direct contribution of instability from the influence on the frontal dynamics of regions with weak stability. This is illustrated in Figure 8.

This continuum can also be interpreted as a succession of behaviour in that, for example, reducing the stability to slantwise convection increases the strength and reduces the scale of slantwise flow, all other things being equal. Whether this full range of behaviour constitutes a SJ may, to some extent, depend on the criteria adopted to identify a SJ. Furthermore, there is no *a priori* reason to suppose that one mechanism operating in one cyclone is necessarily weaker or stronger than a different one operating in another, and

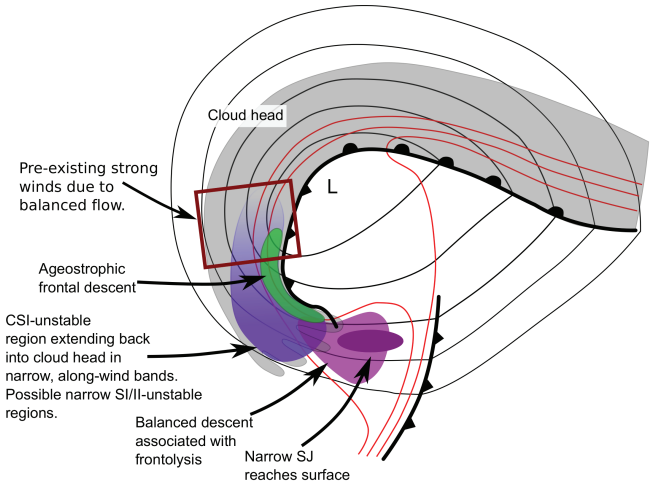

FIGURE 8 Conceptual model of the structure of a SK cyclone at stage II–III of development. The black and red contours are illustrative contours of mean sea level pressure and low-level (e.g. 850 hPa) θ_w, respectively. The surface SJ region can include multiple spatially and temporally distinct wind maxima. Section 9 gives further explanation

there are clear examples where frontolytic descent alone in one system has been associated with wind speeds larger than CSI/SI-enhanced winds in another. "All other things being equal" is a condition that is very difficult (or even impossible) to achieve in practice in all but the most idealized studies. We conclude that it is very difficult to suggest a threshold wind speed to distinguish a SJ based on mechanism, though such a threshold may be useful for more practical purposes.

6 | ROLE OF THE BOUNDARY LAYER

The descending SJ results in strong wind speeds near the top of the boundary layer in all simulated and observed cases. The impact on surface winds and gusts depends on boundary-layer processes that lead to downwards momentum transfer. Analysis of model output and observations has shown that multiple descending jets can occur, leading to multiple near-boundary-layer-top wind maxima; additionally, the high momentum air associated with each wind maxima can be transferred to the surface within multiple convective circulations. For example, Browning *et al.* (2015) diagnosed three types of convective circulations that led to the transfer of momentum from the SJ, either through the jet associated with the CCB or directly to the surface, in the St Jude's Day windstorm: (a) longitudinal rolls of convection in the boundary layer, (b) upper-level or elevated convection and (c) irregular longitudinal rolls of penetrative convection.

Model simulations of both real and idealized cyclones have consistently shown a layer of enhanced static stability forms beneath the descending SJ, typically separating it from the CCB jet below, inhibiting transfer. For example, Baker *et al.* (2014) show layers of positive moist static stability lying between the SJ and CCB in comparable cross-sections through both their idealized cyclone and windstorm *Gudrun*, and Browning *et al.* (2015) show a stable layer between the SJ and CCB jet in model profiles of the St Jude's Day storm. Parton *et al.* (2009) show a layer of air with high-valued dry PV, which would be consistent with similarly high stability, between the SJ and CCB of windstorm *Jeanette*. In their idealized study, Coronel *et al.* (2016) found a layer of strong moist static stability separated descending motions originating in the free troposphere from those originating in the boundary layer towards the leading tip of the SJ, whereas further back, where the stability was weaker and surface winds were stronger, air could descend from about 2 km to the surface.

B04 speculated that reduced static stability may be created by evaporative cooling of air leaving the cloud-head tip, enabling turbulence in the resultant low Richardson number environment or contributing to the triggering of upright convection in a region characterized by potential instability. He provided no direct evidence of this, but the hypothesis was supported by the model simulations of Clark *et al.* (2005) which showed that, once the SJ reached the top of the boundary layer ahead of the CCB in this storm, the vertical profile had constant θ_w (consistent with the SJ flow occurring in the frontal-fracture region) and so was neutrally stable to moist convection. If the boundary layer was cloudy (as it was in the modelled and observed storm), the momentum may have been transferred downwards quite easily. The model simulations clearly show much stronger surface gusts in the SJ region than in either the CCB or WCB region, despite similar wind speeds at 850–900 hPa, consistent with more efficient downward mixing.

In the St Jude's Day storm, Browning *et al.* (2015) showed evidence that both actively precipitating clouds within the SJ and non-precipitating convection in the boundary layer were responsible for the transport of high-momentum air from the SJ to the surface and also diagnosed low Richardson number values within 300 m of the surface where the SJ lay above the CCB jet. They also argue that evaporative cooling led to a reduction of static stability "compared with what the static stability would have been in the presence of unmitigated adiabatic warming of the descending SJ" and so enabled the development of the convective circulations that brought the SJ air with large momentum towards the surface. This quote resolves the apparent contradiction between the B04 study and the later studies reviewed above which showed a layer of enhanced static stability formed beneath the descending SJ. More recently, Slater *et al.* (2017) demonstrated (in a simulation of windstorm *Tini*) that, as expected, the primary role of surface fluxes in the frontal-fracture region is to enhance the downward mixing of momentum from above the boundary layer to the surface southwest of the cyclone centre by reducing the static stability. However, they also suggest that the reduction in boundary-layer static stability reduces the downward advection of air with large values of along-flow momentum, potentially limiting the horizontal extent of the near-surface strong wind region where the boundary layer is unstable.

As discussed above, Hewson and Neu (2015) do not identify SJs directly, but infer their presence from other diagnostics. However, this includes direct observation of surface winds. They compared the boundary-layer stability over land in the regions of strong surface winds associated with a CCB, WCB and SJ. Observational soundings were used for the WCB and CCB jets, but model soundings were used for the SJ due to a lack of a suitable observational sounding; the sample soundings were from different (autumn/winter) storms for each jet, with the SJ analysis from windstorm *Ulli*. The boundary layer was stable at low levels for the CCB and WCB jet, inhibiting downward momentum transfer (though it is noted that over the ocean the boundary layer is more likely to be unstable in the region of the CCB jet). In contrast, the boundary layer for the SJ was dry statically unstable and dry neutrally stable for the model soundings to the west and east of the SJ, respectively below 920 hPa, suggesting that air with large momentum could have descended unimpeded to the surface from this height. However, 920 hPa is well below the level of the top of the boundary layer, which is at about

825 hPa according to the "east" sounding, and so the question of how high-momentum air penetrates this inversion is not answered by this analysis. It must be emphasized, however, that the model profiles are from models that do not have sufficient resolution to develop SJs. Browning *et al.* (2015) show three model soundings along the axis of the descending SJ for the St Jude's Day windstorm. The SJ lies above a stably capped boundary layer in all three soundings; however, downdraughts within elevated convection within the SJ would have been able to descend to the surface at the locations of the two soundings closest to the tip of the SJ.

An important caveat is that SJs present conditions more extreme than those usually assumed in the parametrization of boundary layers in models. The shear generated as the SJ approaches the top of the boundary layer may be very large and quite rapidly changing. The potential warming during later stages of descent may lead to a layer of high static stability, but it is difficult to predict the Richardson number that may result. It is conceivable that large-amplitude and long-wavelength Kelvin–Helmholtz instability could occur, perhaps itself resulting in cloud formation and a consequent change in stability. The majority of articles cited in this review agree that more studies are required of boundary layer/SJ interactions.

6.1 | Summary of the role of the boundary layer

The stability of the boundary layer controls the relationship between the wind speed in the descending SJ and the surface wind speed and gusts. Modelling studies have shown that the descending SJ can create a layer of enhanced static stability near the top of the boundary layer, particularly above the CCB, that inhibits the high-momentum air from reaching the surface. However, SJs descend into the frontal-fracture regions of cyclones (defined by weak thermal gradients) and the boundary layer here has been found to be neutrally stable to moist convection, implying that large-momentum air can reach the surface once within this layer.

7 | THE CLIMATOLOGY OF STING JETS

The small surface footprint of the SJ (less than about 100 km wide) and high resolution needed for their representation in numerical models present challenges for the generation of a SJ climatology derived from either observations or model output. Consequently, most of the literature on SJs to date consists of analysis of high-profile storms, typically those speculated to have had SJs due to the characteristic banding in their cloud heads. To date there are three published climatologies related to SJs, one derived from observations and two (related) from re-analysis data. All climatologies are for cyclones forming over the North Atlantic.

Parton *et al.* (2010) performed a seven-year climatology of strong mid-tropospheric wind events observed by the vertically pointing MST radar located in Aberystwyth on the west coast of Wales, UK. Of the 117 events recorded, they attributed nine to SJs due to their location to the south of the centre of the parent cyclone and close to the tip of the cloud head hook. The wind feature also needed to be distinct from the background flow and remain coherent for 2–3 h over a depth of at least 1.5 km. The nine events occurred during stages III (three events) or IV (six events) of cyclones following the SK conceptual model (Figure 1). This timing somewhat contradicts the conceptual model shown in Clark *et al.* (2005) (reproduced as Figure 2 here) which presents the SJ as occurring in stages II and III of the SK conceptual model with the CCB either undercutting or merging with the SJ in stage IV. Indeed, most of the SJs diagnosed by Parton *et al.* (2010) in stage IV cyclones are located under cloud (their figure 8g) and some distance behind the cold front, which suggests that they may instead have been associated with CCBs.

The scale of SJs means that they cannot be resolved by low-resolution re-analysis or climate model data. However, it is well known that models can develop convective instabilities even if they have insufficient resolution to physically release the instability – a convection parametrization scheme is needed to remove this instability. A necessary part of such parametrization schemes is a diagnosis scheme (often called a "trigger function"). Following this conceptual idea, Martínez-Alvarado *et al.* (2013) presented a SJ "precursor instability" diagnostic and refined it through analysis of three case-studies, each simulated at two resolutions, only one of which was high enough to resolve SJs. The diagnostic was chosen, at least in part, because it is an integral measure that can be computed at one time. It is based on DSCAPE calculated from mid-levels in the cloud head and is related to the volume of air in the cloud head with negative MPV^*, though the two are not proportional. While the diagnosis identifies air that is actually unstable (as it is in cloud), the DSCAPE is likely to indicate more energy than may be released by slantwise descent since the air is likely to become unsaturated on descent.

Martínez-Alvarado *et al.* (2012) (also Martínez-Alvarado *et al.*, 2014b) used this SJ precursor diagnostic to estimate a climatology of SJ cyclones from analysis of 100 North Atlantic cyclones represented by the ECMWF interim re-analysis (ERA-Interim). They validated the diagnostic in a sample of 15 cyclones taken from the 100 intense cyclones by running and analysing high-resolution model simulations using the re-analysis data as initial and boundary conditions. Note that the sample was not based upon the presence or absence of the precursor. Essentially, the high-resolution simulations were examined to establish whether low-level jets could be found in the frontal fracture region that had originated (through trajectory analysis) at mid-levels in the cloud head. The authors required a wind speed in the descending air exceeding 35 m/s to identify a SJ. They showed that SJs could be explicitly identified in the high-resolution simulations in six cases of which

five possessed the SJ precursor diagnostic in the re-analysis, while only two of the remaining nine possessed this diagnostic (but rather weakly). In other words, when the SJ precursor diagnostic is viewed as a predictor, five SJs were confirmed among the seven positive cases, while one SJ was missed in the remaining eight negative cases. Thus, the diagnostic appears to be a very good, if not 100% reliable, indicator of the likely presence of a SJ if a high-resolution model were to be run using the re-analysis data.

This study also provides additional evidence that moist symmetric instability in the cloud head is strongly associated with strong SJs. The authors did not examine frontolysis explicitly. If sufficiently strong SJs exist driven by frontolysis alone, then they would not be diagnosed by this diagnostic. However, the authors clearly expected to see descent in this region even where no strong SJ was present and the methodology would identify SJs in the high-resolution simulations whether the precursor diagnostic was positive or not. One case did occur which met the SJ criterion in the high-resolution simulations despite not showing the precursor diagnostic. However, if these 15 cyclones are added to the total of SJs studied, it would appear that, at the very least, strong SJs driven by frontolysis alone are significantly rarer than those associated with CSI in the cloud head.

Martínez-Alvarado *et al.* (2012) found that between 23 and 32 of the 100 North Atlantic cyclones in the re-analysis had a SJ precursor (dependent on the size of the precursor region required), implying that SJs occur frequently in cyclones, even though they cause damaging surface gusts over land more rarely. While these cyclones generally followed tracks along the main North Atlantic storm track, they all originated south of 50°N, unlike cyclones without the precursors, suggesting that the incorporation of warm moist air may be important (consistent with a role for the release of types of convective instability). Cyclones which originate further south are also more likely to cross the baroclinic jet (from the warm to the cold side); this has been shown to lead to the development of the SK structure favourable for SJ formation (Rivière *et al.*, 2015b) and to the formation of SJs in an idealized modelling study (Coronel *et al.*, 2016).

Hart *et al.* (2017) extended the Martínez-Alvarado *et al.* (2012) methodology to use all suitable cyclones from ERA-Interim data over 33 extended winter seasons from 1979 to 2012. The same SJ precursor diagnostic as Martínez-Alvarado et al. was used, apart from two small changes. In the first, to improve efficiency, the RH criterion was applied before calculating DSCAPE rather than after. This should not affect the results. In the second, a minimum of eight model grid volumes rather than five was used as a more conservative estimate of the importance of sting jet cyclones for wind risk – using the original threshold increases the number of explosively developing storms identified as having the precursor by 29%. Of the 5 447 cyclones tracked, 32% had the SJ precursor (42% in the 22% of cyclones that developed explosively). Precursor storms were found to have a more southerly and zonal storm track than storms without the precursor, and precursor storms tended to be more intense as defined by 850 hPa relative vorticity. It is not possible to estimate how much the SJ would have added to the wind speeds resolved by the re-analysis data, but this study also shows that storms with the SJ precursor diagnostic are the dominant cause of cyclone-related resolved strong wind events over the British Isles, defined as resolved 850 hPa wind speeds exceeding 30 m s^{-1}. However, over continental northwestern Europe, precursor-cyclone-related windstorm events occur far less often.

To date, there have been no studies (of individual cases or climatologies) of SJs in other areas. Mass and Dotson (2010) in their analysis of the climatology of cyclones over the northwest US conclude that, while it is possible that the SJ mechanism could exist in cyclones here, there is "little evidence of its importance" based on a lack of (a) mesoscale localization of strong wind regions, (b) the characteristic cloud-head structure associated with SJ cyclones and (c) SJ features in high-resolution simulations that produce realistic wind speeds. However studies are needed, particularly in the North Pacific storm track.

7.1 | Summary of the climatology of sting jets

The small spatial and short temporal scales of SJs make it difficult to generate climatologies of SJs and the storms in which they occur. The published climatologies to date are of North Atlantic cyclones; however, there is no suggestion that the SJ cyclones are, or environmental reasons to believe that they could be, unique to the atmosphere above this ocean basin. The implication of the climatologies and knowledge of SJ case-studies is that SJs occur frequently in cyclones (in perhaps up to a third of cyclones) and have a major role in strong windstorms over the British Isles, but that they are the direct cause of strong surface winds and gusts over continental northwestern Europe rarely.

8 | MYTHS AND MISUNDERSTANDINGS

In this section we list and explain eight myths and misunderstandings related to SJs which commonly occur based on published literature and other sources such as discussions, presentations at conferences and through reviewing submitted articles.

1. **Myth: Strong near-surface winds in the cool sector of a cyclone are always due to a SJ.**
   Truth: Strong near-surface winds in this region frequently (probably typically) have another cause.
   The CCB jet is an almost universal feature of strongly developing cyclone with a cloud head (e.g. schematics in figures 5.2.62–5.2.64 of Bader *et al.*, 1995). Also, SJs and CCB jets are not the only cause of strong near-surface

winds in the cool sectors of cyclones (i.e. behind the cold front). For example, in these cool sectors, B04 also observed localized strong surface gust regions associated with shallow non-precipitating cloud and Parton *et al.* (2010) observed mid-tropospheric strong wind events attributed to tropopause folds.

2. **Myth: The two possible causes of strong near-surface winds in the cool sector are *either* a SJ *or* a CCB jet, *but not both*.**
   Truth: A SJ may sometimes exist in addition to a CCB jet in strongly developing cyclones.
   The CCB is synoptic-scale flow feature and evolves during the cyclone life cycle (Rivière *et al.*, 2015b). In contrast, the SJ occurs in only some strongly developing cyclones (Martínez-Alvarado *et al.*, 2012) and the descending flows within it are transient, mesoscale features. While the CCB was one of the causes of the strongest wind gusts *over land* in nearly all of the 29 storms analysed in Hewson and Neu (2015) (their table 1), a SJ was considered to be one of the probable or very probable causes in only 13 of the cases. For windstorm *Ulli*, Smart and Browning (2014) found that the SJ was responsible for stronger surface gusts than the CCB jet only for about 2 h, prior to the CCB jet undercutting the SJ.
3. **Myth: SJs can be represented by re-analysis data or coarse resolution climate models.**
   Cao (2009) attribute strong surface winds in at the tip of the bent-back front and cloud head in an idealized cyclone to a SJ. However, the resolution of the model (50 km grid spacing with only 14 model levels) is too coarse to resolve these mesoscale jets and it is highly likely that the simulated strong winds have a different origin. (Trajectory calculation would be needed to identify the cause of this wind feature.)
   Truth: As described in section 4.3, resolution with horizontal grid spacing of about 10–15 km or better with sufficient mid-tropospheric vertical resolution to resolve slantwise descending motions (200–300 m level spacing or better) is required to simulate SJs directly, though a diagnostic for use in coarse-resolution data based on DSCAPE has been developed to identify the cyclones likely to develop a SJ.
4. **Myth: SJs are caused by the transfer of momentum downwards from the upper-tropospheric jet.**
   For example, Baatsen *et al.* (2015) describe as a SJ strong winds at the "end of the back-bent front" attributed to the momentum transport downwards from the jet stream. Schultz and Browning (2017) cite online articles that perpetuate this myth.
   Truth: While this mechanism may cause strong near-surface winds, backwards trajectory analysis reveals that SJ trajectories begin their descent in moist mid-tropospheric air within the cloud head and that the air accelerates as it descends; the origin of the air is thus not the upper-tropospheric jet and, while it may start in the cloud head with already high speed, this increases during descent.
   Strong surface winds have been associated with descending stratospheric intrusions and, more generally, dry intrusions in case-studies and a climatology (Browning and Reynolds, 1994; Raveh-Rubin, 2017). However, Parton *et al.* (2010) distinguish mid-tropospheric strong wind events associated with tropopause folds (and by implication the baroclinic jet) from those associated with SJs in their observational analysis, and show that these strong events occur in different places relative to the cyclone. (Slater *et al.*, 2015) find an airstream resembling a dry intrusion descended into the strong near-surface wind region to the southwest of the cyclone centre from the west in their dry idealized cyclone. This airstream was distinct from the other main airstream entering this region which the authors identify as the CCB. Finally, dropsonde observations and model simulations from windstorm *Friedhelm* show the wind maximum associated with the dry intrusion is well-separated from the lower-level wind maximum associated with the SJ (Martínez-Alvarado *et al.*, 2014a).
5. **Myth: SJs can exist in dry idealized cyclones.**
   (Slater *et al.*, 2015) describe a set of "transitional trajectories" following paths between those of the trajectories following the CCB and dry intrusion in their dry idealized cyclone as resembling a SJ. Due to their transitional nature, these trajectories descend while following a cyclonic path around the low centre, a path similar to that followed by diagnosed SJs in case-studies. Though there is likely to be weakly descending air in this region for the reasons identified that article, there is no evidence that this airstream is distinct from the two other airstreams and associated with a distinct wind maximum (i.e. no actual distinct jet was identified). The single trajectory shown is likely to be simply an intermediate behaviour trajectory between two neighbours. Hence, a SJ, as defined in section 4.4, did not form in this cyclone.
   Truth: There is no evidence that SJs can form in dry cyclones and indeed plenty of evidence that moist processes are important.
   Baker *et al.* (2014) simulated a SJ feature in a moist idealized cyclone (12 km horizontal grid spacing with 200–300 m mid-tropospheric level spacing), whereas in a corresponding dry simulation the frontal-fracture region was less distinct with no associated local wind maxima that could be attributed to a SJ.
6. **Myth: If a SJ exists then it is the cause of the strongest surface winds and gusts in the cyclone.**
   Truth: Often the CCB jet produces the strongest winds and gusts.
   In the Great Storm the strongest surface gusts were associated with the SJ (the gusts reached about 30 and 45 m s^{-1} in the CCB and SJ regions, respectively) and the SJ impacted surface winds ahead of the CCB jet. However,

in other case-studies, such as windstorms *Ulli* (Smart and Browning, 2014) and *Gudrun* (Baker, 2009), the strongest gusts were attributed to the CCB jet. Since the SJ descends from the mid-troposphere towards the top of the boundary layer, the resulting surface wind gusts are critically dependent on the boundary-layer stability (section 6). Furthermore, in some cases, the SJ may descend above the CCB but not extend beyond it. In this case, it is possible that the SJ influences the CCB winds.

7. **Myth: Cyclones containing SJs can be found only in the eastern North Atlantic and western Europe.**
   To date, to the authors' knowledge, there have been no case-studies and climatologies of SJ cyclones outside this region, especially over the Pacific storm track. All the published studies relate to cyclones in this region. Mass and Dotson (2010) in their analysis of the climatology of cyclones over the northwest US conclude that there is little evidence of the SJ mechanism.
   Truth: The current lack of verified SJ cyclones beyond the eastern North Atlantic and western Europe does not, of course, mean that they do not exist, but more research is needed to assess their global climatology.
   The successful simulation of these cyclones in idealized simulations (Baker *et al.*, 2014; Coronel *et al.*, 2016) implies that SJs can exist wherever cyclones evolve following the SK evolution; section 2.1 suggests that such cyclones may preferentially exist near the entrance, rather than the exit, of the storm tracks. They may also preferentially occur in cyclones that have their origins in the Subtropics (Martínez-Alvarado *et al.*, 2012). Also, as discussed above, a SJ need not be responsible for the strongest wind gusts in a given storm and, especially in the presence of high orography, its presence may not be diagnosable from surface observations. Finally, reports do exist outside of peer-reviewed journals of possible SJ cyclones observed in other parts of the world (e.g. Doyle and Mo, 2015).
8. **Myth: Only one mechanism for the descent and speed-up of an SJ in cyclones must exist, and there is a conflict over whether this is either CSI release or frontal (or geostrophic) forcing. If one mechanism is shown to occur in one cyclone, it must therefore be the "right" mechanism for all SJs.**
   Truth: While more research is needed here, a continuum of behaviour is likely to occur as described in section 5.7.
   While Browning (in B04) recognised that the SJ occurred in a region of general descent in the frontal-fracture region of cyclones and that balanced dynamics accounted for most of the wind strength, he also speculated that mesoscale processes such as CSI release and evaporation could enhance it. Consequently, many of the articles following B04 focused on the assessment of the role of CSI release and evaporation (e.g. Parton *et al.*, 2009; Gray *et al.*, 2011). There now seems to be a substantial body of evidence that strong SJs often originate from regions of the cloud head unstable to CSI or even SI or II, and that this instability is released as the SJ develops.

   Some more recent articles have instead directly assessed the role of frontolysis (Schultz and Sienkiewicz, 2013), the synoptic-scale geostrophic forcing (Coronel *et al.*, 2016) or both (Slater *et al.*, 2017) in leading to descent in this frontal-fracture region and proposed these as alternative mechanisms for SJ descent. For example, Schultz and Sienkiewicz (2013) state that "Thus, descent associated with the frontolysis reaching a near-neutral boundary layer provides a physical mechanism for SJs, is consistent with previous studies, and synthesizes existing knowledge."
   This re-emphasises the role of balanced dynamics in promoting the descent of strong winds from the cloud head.

   Thus, the choice is not between frontolysis and mesoscale instability. The former is likely to be ubiquitous in the frontal fracture region, though may be stronger in some cyclones. The nature of the resulting flow is likely to be modified by the degree of stability, becoming more jet-like as a system approaches neutral stability, and generating multiple, more intense, jets as a system becomes unstable. In practice, it is very difficult to separate the contribution of mesoscale instability from the larger-scale frontolysis process.

   The apparent conflict also likely arises in some articles, in part, due to confusion over the definition of a SJ compounded with some of the myths above (especially regarding the CCB). As described in section 4.4, a SJ must descend from the cloud-head tip (verification of this typically requires trajectory analysis using model output); the presence of strong near-surface winds in the frontal-fracture region of a cyclone does not automatically imply a SJ. Future work should recognise the continuum of processes leading to strong winds in the cool sector of cyclones.

9 | CONCLUSIONS

Since the pioneering paper of B04, SJs and their associated cyclones have been the subject of an increasing number of journal articles and the term has entered the public domain (e.g. the BBC television weather forecast of windstorm *Ulli*); also Schultz and Browning, 2017). As the evidence has emerged that SJs are a feature of many extreme windstorms affecting northern Europe and understanding of this phenomenon has increased, some misunderstandings have entered the literature. The mechanism(s) causing the descent and acceleration of the SJ air has also been a subject of some debate. In this review we have attempted to provide a complete history of the "sting-jet era," provide a consistent

definition of a SJ (section 9.1) and consolidate the knowledge learnt, in particular regarding mechanisms (section 9.2). The interaction between the atmospheric boundary layer and SJs and the global climatology of SJs are revealed as specific areas where more research is needed. We have ended this article with a list of myths and misunderstandings that we have encountered in our reading of the published literature and discussions with colleagues. We hope that this list will be of particular use to researchers new to this area of research.

9.1 | Definition of a sting jet

The SJ is defined as a coherent airflow that descends from mid-levels inside the cloud head into the frontal-fracture region of a SK cyclone over a period of a few hours leading to a distinct region of near-surface stronger winds. It lies above the CCB during some stage of its life, but, at least in some cases, descends to reach the top of the boundary layer ahead of the CCB. Strong near-surface wind speeds and gusts may or may not result from a SJ depending on boundary-layer processes. It is not attributed to a specific mechanism in this definition.

SJs do not, in all cases, accelerate beyond the tip of the CCB, so may not always form a distinct peak in speed at the surface, though it seems likely that, in this case, the SJ may still enhance the impact of the CCB. Figure 7 illustrates the spatial relationship to the CCB and WCB.

9.2 | Summary of mechanisms

We conclude that it is likely that a continuum of SJ descent and speed-up mechanisms exists. This is illustrated in Figure 8. Balanced descent associated with frontolysis in the frontal-fracture region produces a broad region of air in the cloud head, with already relatively strong horizontal speed, descending into the frontal-fracture region where it can experience stronger along-wind pressure gradients. More horizontally small-scale and stronger frontolytic descent may, in some circumstances, occur due to weak stability to slantwise convective downdraughts, possibly enhanced by cooling by evaporation or sublimation of hydrometeors falling from the upper part of the cloud head. In extreme cases the release of conditional symmetric instability and even symmetric instability can result is stronger descent and further enhanced near-surface wind speed. In these cases multiple slantwise convective downdraughts may occur.

These mechanisms are presented as a succession only in the sense that, broadly speaking, in a given storm each stage tends to enhance the focus of the jet and increase its speed; but it appears to be possible that some storms exhibiting only the first mechanism may produce winds stronger than in some other storms exhibiting the full range. Furthermore, as noted above, SJs may exist in some storms that are weaker than the CCB.

ACKNOWLEDGEMENTS

The authors have benefited from energetic discussions with many colleagues regarding the nature and evidence for SJs. In particular, we would like to thank Oscar Martínez-Alvarado, Neil Hart, Laura Baker, Ambrogio Volonté, John Methven, Geraint Vaughan and David Schultz. We would also like to thank Neil Hart for his sketch that inspired Figure 7. We also thank Gwendal Rivière and an anonymous reviewer for insightful comments which have improved this review. This work was part funded by the Natural Environment Research Council funded project "Sting jets in severe Northern European windstorms" (NE/E004415/1) and the AXA Research Fund project "Sting jet windstorms in current and future climates."

ORCID

Peter A. Clark http://orcid.org/0000-0003-1001-9226

REFERENCES

Baatsen, M., Haarsma, R.J., van Delden, A.J. and de Vries, H. (2015) Severe Autumn storms in future Western Europe with a warmer Atlantic Ocean. *Climate Dynamics*, 45, 949–964. https://doi.org/10.1007/s00382-014-2329-8.

Bader, M.J., Forbes, G.S., Grant, J.R., Lilley, R.B.E. and Waters, A.J. (1995) *Images in Weather Forecasting*. Cambridge: Cambridge University Press.

Baker, L.H. (2009) Sting jets in severe Northern European wind storms. *Weather*, 64, 143–148. https://doi.org/10.1002/wea.397.

Baker, L.H., Gray, S.L. and Clark, P.A. (2014) Idealized simulations of sting-jet cyclones. *Quarterly Journal of the Royal Meteorological Society*, 140, 96–110. https://doi.org/10.1002/qj.2131.

Baker, L.H., Martínez-Alvarado, O., Methven, J. and Knippertz, P. (2013) Flying through extratropical cyclone *Friedhelm*. *Weather*, 68, 9–13. https://doi.org/10.1002/wea.2047.

Bennetts, D.A. and Hoskins, B.J. (1979) Conditional symmetric instability – a possible explanation for frontal rainbands. *Quarterly Journal of the Royal Meteorological Society*, 105, 945–962. https://doi.org/10.1002/qj.49710544615.

Bjerknes, J. (1919) On the structure of moving cyclones. *Geofysiske Publikationer*, 1, 1–8.

Bjerknes, J. and Solberg, H. (1922) Life cycles of cyclones and the polar front theory of atmospheric circulation. *Geofysiske Publikationer*, 3, 1–18.

Böttger, H., Eckardt, M. and Katergiannakis, U. (1975) Forecasting extratropical storms with hurricane intensity using satellite information. *Journal of Applied Meteorology*, 14, 1259–1265.

Browning, K.A. (1971) Radar measurements of air motion near fronts. *Weather*, 26, 320–340.

Browning, K.A. (2004) The sting at the end of the tail: damaging winds associated with extratropical cyclones. *Quarterly Journal of the Royal Meteorological Society*, 130, 375–399. https://doi.org/10.1256/qj.02.143.

Browning, K.A. (2005) Observational synthesis of mesoscale structures within an explosively developing cyclone. *Quarterly Journal of the Royal Meteorological Society*, 131, 603–623. https://doi.org/10.1256/qj.03.201.

Browning, K.A. and Field, M. (2004) Evidence from Meteosat imagery of the interaction of sting jets with the boundary layer. *Meteorological Applications*, 11, 277–289. https://doi.org/10.1017/S1350482704001379.

Browning, K.A. and Reynolds, R. (1994) Diagnostic study of a narrow cold-frontal rainband and severe winds associated with a stratospheric intrusion. *Quarterly Journal of the Royal Meteorological Society*, 120, 235–257. https://doi.org/10.1002/qj.49712051602.

Browning, K.A. and Roberts, N.M. (1994) Structure of a frontal cyclone. *Quarterly Journal of the Royal Meteorological Society*, 120, 1535–1557.

Browning, K.A., Clough, S.A., Davitt, C.S.A., Roberts, N.M., Hewson, T.D. and Healey, P.G.W. (1995) Observations of the mesoscale sub-structure in the cold

air of a developing frontal cyclone. *Quarterly Journal of the Royal Meteorological Society*, 121, 1229–1254. https://doi.org/10.1002/qj.49712152604.

Browning, K.A., Chapman, D. and Dixon, R.S. (2001) Stacked slantwise convective circulations. *Quarterly Journal of the Royal Meteorological Society*, 127, 2513–2536. https://doi.org/10.1002/qj.49712757803.

Browning, K.A., Smart, D.J., Clark, M.R. and Illingworth, A.J. (2015) The role of evaporating showers in the transfer of sting-jet momentum to the surface. *Quarterly Journal of the Royal Meteorological Society*, 141, 2956–2971. https://doi.org/10.1002/qj.2581.

Cao, Z. (2009) The sting jet in a simulated extratropical cyclone. *The Open Atmospheric Science Journal*, 3, 212–218.

Carlson, T.N. (1980) Airflow through midlatitude cyclones and the comma cloud pattern. *Monthly Weather Review*, 108, 1498–1509.

Clark, P.A., Browning, K.A. and Wang, C. (2005) The sting at the end of the tail: model diagnostics of the fine-scale three-dimensional structure of the cloud band. *Quarterly Journal of the Royal Meteorological Society*, 131, 2263–2292. https://doi.org/10.1256/qj.04.36.

Clough, S.A. and Franks, R. (1991) The evaporation of frontal and other stratiform precipitation. *Quarterly Journal of the Royal Meteorological Society*, 117, 1057–1080. https://doi.org/10.1002/qj.49711750109.

Coronel, B., Ricard, D., Rivière, G. and Arbogast, P. (2016) Cold-conveyor-belt jet, sting jet and slantwise circulations in idealized simulations of extratropical cyclones. *Quarterly Journal of the Royal Meteorological Society*, 142, 1781–1796. https://doi.org/10.1002/qj.2775.

Deardorff, J. (1980) Stratocumulus-capped mixed layers derived from a three-dimensional model. *Boundary-Layer Meteorology*, 18, 495–527.

Doyle, C. and Mo, R. (2015) *A rather rare West Coast sting-jet event during December 12–13, 2015*. Vancouver: National Laboratory for Coastal and Mountain Meteorology, Environment and Climate Change Canada. Technical Report: 2015–001.

Ducrocq, V. (1993) Adiabatic and viscous simulations of symmetric instability: structure, evolution and energetics. *Journal of Atmospheric Sciences*, 50, 23–42.

Eliassen, A. (1962) On the vertical circulation in frontal zones. *Geofysisker Publikationer*, 24(4), 147–160.

Emanuel, K.A. (1983) The Lagrangian parcel dynamics of moist symmetric instability. *Journal of Atmospheric Sciences*, 40, 2368–2376. https://doi.org/10.1175/1520-0469(1983)040<2368:tlpdom>2.0.CO;2.

Emanuel, K. (1985) Frontal circulations in the presence of small moist symmetric stability. *Journal of Atmospheric Sciences*, 42, 1062–1071.

Fischer, C. and Lalaurette, F. (1995) Meso-scale circulations in realistic fronts. I: steady basic state. *Quarterly Journal of the Royal Meteorological Society*, 121, 1255–1283. https://doi.org/10.1002/qj.49712152605.

Forbes, R.M. and Clark, P.A. (2003) Sensitivity of extratropical cyclone mesoscale structure to the parametrization of ice microphysical processes. *Quarterly Journal of the Royal Meteorological Society*, 129, 1123–1148. https://doi.org/10.1256/qj.01.171.

Fox, A., Sherwin, R. and Ralston, F. (2012) Lessons learnt at the Met Office from the Great Storm of 1987. *Weather*, 67, 268–273. https://doi.org/10.1002/wea.1981.

Gray, S.L. and Thorpe, A.J. (2001) Parcel theory in three dimensions and the calculation of SCAPE. *Monthly Weather Review*, 129, 1656–1672. https://doi.org/10.1175/1520-0493(2001)129<1656:ptitda>2.0.CO;2.

Gray, S.L., Martínez-Alvarado, O., Baker, L.H. and Clark, P.A. (2011) Conditional symmetric instability in sting jet storms. *Quarterly Journal of the Royal Meteorological Society*, 137, 1482–1500. https://doi.org/10.1002/qj.859.

Grayson, A.J. (1989) *The 1987 Storm: Impacts and Responses*, Bulletin 87. Edinburgh: Forestry Commission.

Grønås, S. (1995) The seclusion intensification of the New Year's Day storm 1992. *Tellus A*, 47, 733–746. https://doi.org/10.1034/j1600-08701995.00116.X.

Harrold, T.W. (1973) Mechanisms influencing the distribution of precipitation within baroclinic disturbances. *Quarterly Journal of the Royal Meteorological Society*, 99, 232–251.

Hart, N.C.G., Gray, S.L. and Clark, P.A. (2017) Sting-jet windstorms over the North Atlantic: climatology and contribution to extreme wind risk. *Journal of Climate*, 30, 5455–5471. https://doi.org/10.1175/JCLI-D-16-0791.1.

Haynes, P.H. and McIntyre, M.E. (1987) On the evolution of vorticity and potential vorticity in the presence of diabatic heating and frictional or other forces. *Journal of Atmospheric Sciences*, 44, 828–841. https://doi.org/10.1175/1520-0469(1987)044<0828:oteova>2.0.CO;2.

Hewson, T.D. and Neu, U. (2015) Cyclones, windstorms and the IMILAST project. *Tellus A*, 67, 27–128. https://doi.org/10.3402/tellusa.v67.27128.

Holt, M.W. and Thorpe, A.J. (1991) Localized forcing of slantwise motion at fronts. *Quarterly Journal of the Royal Meteorological Society*, 117, 943–963.

Holton, J.R. (2004) *An Introduction to Dynamic Meteorology*, 4th edition. Cambridge, MA: Elsevier Academic Press.

Hoskins, B.J. (1974) The role of potential vorticity in symmetric stability and instability. *Quarterly Journal of the Royal Meteorological Society*, 100, 480–482. https://doi.org/10.1002/qj.49710042520.

Hoskins, B.J., Draghici, I. and Davies, H.C. (1978) A new look at the omega equation. *Quarterly Journal of the Royal Meteorological Society*, 104, 31–38. https://doi.org/10.1002/qj.49710443903.

Huang, H.C. and Emanuel, K.A. (1991) The effects of evaporation on frontal circulation. *Journal of Atmospheric Sciences*, 48, 619–628.

Jones, S.C. and Thorpe, A.J. (1992) The three-dimensional nature of 'symmetric' instability. *Quarterly Journal of the Royal Meteorological Society*, 118, 227–258. https://doi.org/10.1002/qj.49711850404.

Knapp, K.R., Ansari, S., Bain, C.L., Bourassa, M.A., Dickinson, M.J., Helms, C.F.C.N., Magnusdottir, G., Holmes, C.D., Huffman, G.J., Kossin, J.P., Lee, H.T., Loew, A. and Hennon, C.C. (2011) Globally gridded satellite (GridSat) observations for climate studies. *Bulletin of the American Meteorological Society*, 92, 893–907. https://doi.org/10.1175/2011BAMS3039.1.

Koch, P., Wernli, H. and Davies, H.C. (2006) An event-based jet-stream climatology and typology. *International Journal of Climatology*, 26, 283–301. https://doi.org/10.1002/joc.1255.

Lean, H.W. and Clark, P.A. (2003) The effects of changing resolution on mesocale modelling of line convection and slantwise circulations in FASTEX IOP16. *Quarterly Journal of the Royal Meteorological Society*, 129, 2255–2278. https://doi.org/10.1256/qj.02.57.

Leckebusch, G.C., Renggli, D. and Ulbrich, U. (2008) Development and application of an objective storm severity measure for the Northeast Atlantic region. *Meteorologische Zeitschrift*, 17, 575–587. https://doi.org/10.1127/0941-2948/2008/0323.

Lemaître, Y., Scialom, G. and Protat, A. (2001) Conditional symmetric instability, frontogenetic forcing and rain-band organization. *Quarterly Journal of the Royal Meteorological Society*, 127, 2599–2634. https://doi.org/10.1002/qj.49712757806.

Martínez-Alvarado, O., Weidle, F. and Gray, S.L. (2010) Sting jets in simulations of a real cyclone by two mesoscale models. *Monthly Weather Review*, 138, 4054–4075. https://doi.org/10.1175/2010MWR3290.1.

Martínez-Alvarado, O., Gray, S.L., Catto, J.L. and Clark, P.A. (2012) Sting jets in intense North Atlantic windstorms. *Environmental Research Letters*, 7, 024014. https://doi.org/10.1088/1748-9326/7/2/024014.

Martínez-Alvarado, O., Gray, S.L., Clark, P.A. and Baker, L.H. (2013) Objective detection of sting jets in low-resolution datasets. *Meteorological Applications*, 20, 41–55. https://doi.org/10.1002/met.297.

Martínez-Alvarado, O., Baker, L.H., Gray, S.L., Methven, J. and Plant, R.S. (2014a) Distinguishing the cold conveyor belt and sting jet air streams in an intense extratropical cyclone. *Monthly Weather Review*, 142, 2571–2595. https://doi.org/10.1002/met.297.

Martínez-Alvarado, O., Gray, S.L., Catto, J.L. and Clark, P.A. (2014b) Corrigendum: sting jets in intense winter North-Atlantic windstorms (2012 Environmental Research Letters 7, 024014). *Environmental Research Letters*, 9, 039501. https://doi.org/10.1088/1748-9326/9/3/039501.

Mass, C. and Dotson, B. (2010) Major extratropical cyclones of the Northwest United States: historical review, climatology, and synoptic environment. *Monthly Weather Review*, 138, 2499–2527. https://doi.org/10.1175/2010MWR3213.1.

Met Office Advisory Services. (1988) A detailed description of wind and weather during the passage of the storm of 15/16 October 1987 across southern England. *Meteorological Magazine*, 117, 104–109.

Morcrette, C.J. and Browning, K.A. (2006) Formation and release of symmetric instability following Delta-M adjustment. *Quarterly Journal of the Royal Meteorological Society*, 132, 1073–1089. https://doi.org/10.1256/qj.04.108.

Neiman, P.J., Shapiro, M. and Fedor, L. (1993) The life cycle of an extratropical marine cyclone. Part II: mesoscale structure and diagnostics. *Monthly Weather Review*, 121, 2177–2199.

Newton, C.W. and Holopainen, E.O. (Eds.) (1990) *Extratropical Cyclones: The Eric Palmén Memorial Volume*. Boston, MA: American Meteorological Society.

Ooyama, K. (1966) On the stability of the baroclinic circular vortex: a sufficient criterion for instability. *Journal of Atmospheric Sciences*, 23, 43–53. https://doi.org/10.1175/1520-0469(1966)023<0043:otsotb>2.0.CO;2.

Papritz, L. and Schemm, S. (2013) Development of an idealised downstream cyclone: Eulerian and Lagrangian perspective on the kinetic energy. *Tellus A*, 65, 19539. https://doi.org/10.3402/tellusa.v65i0.19539.

Parton, G., Dore, A. and Vaughan, G. (2010) A climatology of mid-tropospheric mesoscale strong wind events as observed by the MST radar, Aberystwyth. *Meteorological Applications*, 17, 340–354. https://doi.org/10.1002/met.203.

Parton, G.A., Vaughan, G., Norton, E.G., Browning, K.A. and Clark, P.A. (2009) Wind profiler observations of a sting jet. *Quarterly Journal of the Royal Meteorological Society*, 135, 663–680. https://doi.org/10.1002/qj.398.

Persson, P.O.G. and Warner, T.T. (1991) Model generation of spurious gravity waves due to inconsistency of the vertical and horizontal resolution. *Monthly Weather Review*, 119, 917–935. https://doi.org/10.1175/1520-0493(1991)119<0917:mgosgw>2.0.CO;2.

Persson, P.O.G. and Warner, T.T. (1993) Nonlinear hydrostatic conditional symmetric instability: implications for numerical weather prediction. *Monthly Weather Review*, 121, 1821–1833. https://doi.org/10.1175/1520-0493(1993)121<1821:nhcsii>2.0.CO;2.

Pinto, J.F., Zacharias, S., Fink, A.H., Leckebusch, G.C. and Ulbrich, U. (2009) Factors contributing to the development of extreme North Atlantic cyclones and their relationship with the NAO. *Climate Dynamics*, 32, 711–737. https://doi.org/0.1007/s00382-008-0396-4.

Pizzamei, M., Gray, S.L. and Browning, K.A. (2005) Cloud-resolving model simulations of multiply-banded frontal clouds. *Quarterly Journal of the Royal Meteorological Society*, 131, 2617–2637. https://doi.org/10.1256/qj.04.175.

Raveh-Rubin, S. (2017) Dry intrusions: Lagrangian climatology and dynamical impact on the planetary boundary layer. *Journal of Climate*, 30, 6661–6682.

Reuter, G.W. and Yau, M.K. (1990) Observations of slantwise convective instability in winter cyclones. *Monthly Weather Review*, 118, 447–458. https://doi.org/10.1175/1520-0493(1990)118<0447:ooscii>2.0.CO;2.

Rivière, G., Arbogast, P. and Joly, A. (2015a) Eddy kinetic energy redistribution within idealized extratropical cyclones using a two-layer quasi-geostrophic model. *Quarterly Journal of the Royal Meteorological Society*, 141, 207–223. https://doi.org/10.1002/qj.2350.

Rivière, G., Arbogast, P. and Joly, A. (2015b) Eddy kinetic energy redistribution within windstorms *Klaus* and *Friedhelm*. *Quarterly Journal of the Royal Meteorological Society*, 141, 925–938. https://doi.org/10.1002/qj.2412.

Roberts, N.M. and Forbes, R.M. (2002) An observational study of multiple cloud head structure in the FASTEX IOP 16 cyclone. *Atmospheric Science Letters*, 3, 59–70. https://doi.org/10.1006/asle.2002.0048.

Sanders, F. and Gyakum, J.R. (1980) Synoptic-dynamic climatology of the "Bomb". *Monthly Weather Review*, 108, 1589–1606. https://doi.org/10.1175/1520-0493(1980)108<1589:sdcot>2.0.CO;2.

Sawyer, J.S. (1956) The vertical circulation at meteorological fronts and its relation to frontogenesis. *Proceedings of the Royal Society*, 234, 346–362. https://doi.org/10.1098/rspa.1956.0039.

Schultz, D.M. (2001) Re-examining the cold conveyor belt. *Monthly Weather Review*, 129, 2205–2225. https://doi.org/10.1175/1520-0493(2001)129<2205:rtccb>2.0.CO;2.

Schultz, D.M. and Browning, K.A. (2017) What is a sting jet? *Weather*, 72, 63–66. https://doi.org/10.1002/wea.2795.

Schultz, D.M. and Schumacher, P.N. (1999) The use and misuse of conditional symmetric instability. *Monthly Weather Review*, 127, 2709–2732. https://doi.org/10.1175/1520-0493(1999)127<2709:tuamoc>2.0.CO;2.

Schultz, D.M. and Sienkiewicz, J.M. (2013) Using frontogenesis to identify sting jets in extratropical cyclones. *Weather and Forecasting*, 28, 603–613. https://doi.org/10.1175/WAF-D-12-00126.1.

Schultz, D.M. and Vaughan, G. (2011) Occluded fronts and the occlusion process: a fresh look at conventional wisdom. *Bulletin of the American Meteorological Society*, 92, 443–466. https://doi.org/10.1175/2010BAMS3057.1.

Schultz, D.M. and Zhang, F. (2007) Baroclinic development within zonally varying flows. *Quarterly Journal of the Royal Meteorological Society*, 133, 1101–1112. https://doi.org/10.1002/qj.87.

Schultz, D.M., Keyser, D. and Bosart, L.F. (1998) The effect of large-scale flow on low-level frontal structure and evolution in midlatitude cyclones. *Monthly Weather Review*, 126, 1767–1791.

Shapiro, M.A. and Grønås, S. (Eds.) (1999) *The Life Cycles of Extratropical Cyclones*. Boston, MA: American Meteorological Society.

Shapiro, M.A. and Keyser, D.A. (1990) Fronts, jet streams, and the tropopause. In: Newton, C.W. and Holopainen, E.O. (Eds.) *Extratropical Cyclones: The Erik Palmén Memorial Volume*. Boston, MA: American Meteorological Society, pp. 167–191.

Shapiro, M.A., Wernli, H., Bao, J.W., Methven, J., Zou, X., Doyle, J., Holt, T., Donall-Grell, E. and Neiman, P. (1999) A planetary-scale to mesoscale perspective of the life cycles of extratropical cyclones: the bridge between theory and observations. In: Shapiro M.A. and Grønås S (Eds.) *The Life Cycles of Extratropical Cyclones*. Boston, MA: American Meteorological Society, pp. 139–185.

Skamarock, W.C., Park, S.H., Klemp, J.B. and Snyder, C. (2014) Atmospheric kinetic energy spectra from global high-resolution nonhydrostatic simulations. *Journal of Atmospheric Sciences*, 71, 4369–4381. https://doi.org/10.1175/JAS-D-14-0114.1.

Slater, T.P., Schultz, D.M. and Vaughan, G. (2015) Acceleration of near-surface strong winds in a dry, idealized extratropical cyclone. *Quarterly Journal of the Royal Meteorological Society*, 1417, 1004–1016. https://doi.org/10.1002/qj.2417.

Slater, T.P., Schultz, D.M. and Vaughan, G. (2017) Near-surface strong winds in a marine extratropical cyclone: acceleration of the winds and the importance of surface fluxes. *Quarterly Journal of the Royal Meteorological Society*, 143, 321–332. https://doi.org/10.1002/qj.2924.

Smart, D.J. and Browning, K.A. (2014) Attribution of strong winds to a cold conveyor belt and sting jet. *Quarterly Journal of the Royal Meteorological Society*, 140, 595–610. https://doi.org/10.1002/qj.2162.

Smith, R.N.B. (1990) A scheme for predicting layer clouds and their water content in a general circulation model. *Quarterly Journal of the Royal Meteorological Society*, 116, 435–460. https://doi.org/10.1002/qj.49711649210.

Thorpe, A.J. and Clough, S.A. (1991) Mesoscale dynamics of cold fronts: structures described by dropsoundings in FRONTS 87. *Quarterly Journal of the Royal Meteorological Society*, 117, 903–941. https://doi.org/10.1002/qj.49711750103.

Thorpe, A.J. and Emanuel, K.A. (1985) Frontogenesis in the presence of small stability to slantwise convection. *Journal of Atmospheric Sciences*, 42, 1809–1824.

Vaughan, G., Methven, J., Anderson, D., Antonescu, B., Baker, L., Baker, T.P., Ballard, S.P., Bower, K.N., Brown, P.R.A., Chagnon, J., Choularton, T.W., Chylik, J., Connolly, P.J., Cook, P.A., Cotton, R.J., Crosier, J., Dearden, C., Dorsey, J.R., Frame, T.H.A., Gallagher, M.W., Goodliff, M., Gray, S.L., Harvey, B.J., Knippertz, P., Lean, H.W., Li, D., Lloyd, G., Martínez-Alvarado, O., Nicol, J., Norris, J., Öström, E., Owen, J., Parker, D.J., Plant, R.S., Renfrew, I.A., Roberts, N.M., Rosenberg, P., Rudd, A.C., Schultz, D.M., Taylor, J.P., Trzeciak, T., Tubbs, R., Vance, A.K., van Leeuwen, P.J., Wellpott, A. and Woolley, A. (2015) Cloud banding and winds in intense European cyclones: results from the DIAMET project. *Bulletin of the American Meteorological Society*, 96, 249–265. https://doi.org/10.1175/BAMS-D-13-00238.1.

Volonté, A., Clark, P.A. and Gray, S.L. (2018) The role of mesoscale instabilities in the sting-jet dynamics of windstorm *Tini*. *Quarterly Journal of the Royal Meteorological Society*. https://doi.org/10.1002/qj.3264.

Wakimoto, R.M., Blier, W. and Liu, C. (1992) The frontal structure of an explosive oceanic cyclone: airborne radar observations of ERICA IOP 4. *Monthly Weather Review*, 120, 1135–1155. https://doi.org/10.1175/1520-0493(1992)120,1135:TFSOAE.2.0.CO;2.

Xu, Q. (1989) Frontal circulations in the presence of small viscous moist symmetric stability and weak forcing. *Quarterly Journal of the Royal Meteorological Society*, 115, 1325–1353. https://doi.org/10.1002/qj.49711549008.

How to cite this article: Clark PA, Gray SL. Sting jets in extratropical cyclones: a review. *Q J R Meteorol Soc.* 2018;144:943–969. https://doi.org/10.1002/qj.3267